Journal of Visualized Experiments

Two-Dimensional Visualization and Quantification of Labile, Inorganic Plant Nutrients and Contaminants in Soil

--Manuscript Draft--

Article Type:	Invited Methods Article - JoVE Produced Video
Manuscript Number:	JoVE61661R1
Full Title:	Two-Dimensional Visualization and Quantification of Labile, Inorganic Plant Nutrients and Contaminants in Soil
Section/Category:	JoVE Environment
Keywords:	Chemical imaging; Rhizosphere; diffusive gradients in thin films; laser ablation inductively coupled plasma mass spectrometry; trace element; plant nutrition
Corresponding Author:	Jakob Santner Universitat fur Bodenkultur Department fur Nutzpflanzenwissenschaften Tulln, Lower Austria AUSTRIA
Corresponding Author's Institution:	Universitat fur Bodenkultur Department fur Nutzpflanzenwissenschaften
Corresponding Author E-Mail:	jakob.santner@boku.ac.at
Order of Authors:	Stefan Wagner
	Christoph Hoefer
	Thomas Prohaska
	Jakob Santner
Additional Information:	
Question	**Response**
Please indicate whether this article will be Standard Access or Open Access.	Standard Access (US$2,400)
Please indicate the **city, state/province, and country** where this article will be **filmed**. Please do not use abbreviations.	Tulln an der Donau, Austria

Dear Editor,

herewidth we submit a protocol on nutrient and contaminant imaging in plant rhizospheres. The method described in this manuscript is an advanced technique for visualising and quantifying multiple inorganic nutrient and/or contaminant species around roots growing. We look forward to a positive response and constructive comments from you and the reviewers after review.

I would like to ask you to not select Prof. Shiming Ding as a reviewer for this manuscript. We are having scientific disputes with Prof. Ding, which unfortunately have not always remained within the boundaries of fair evaluation of scientific results. I also do not accept review assignments of the work of Prof. Ding anymore in order to maintain scientific neutrality.

Prof. Shiming Ding

smding@niglas.ac.cn

Chinese Academy of Sciences

Department Lake Sciences and Engineering

Beijing, China

Best regards

Jakob Santner

TITLE:

Two-Dimensional Visualization and Quantification of Labile, Inorganic Plant Nutrients and Contaminants in Soil

AUTHORS AND AFFILIATIONS:

Stefan Wagner[1], Christoph Hoefer[2], Thomas Prohaska[1], Jakob Santner[1,3]

[1]Department General, Analytical and Physical Chemistry, Chair of General and Analytical Chemistry, Montanuniversität Leoben, Franz-Josef-Straße, Leoben, Austria.
[2]Department of Forest and Soil Sciences, Institute of Soil Research, Rhizosphere Ecology and Biogeochemistry Group, University of Natural Resources and Life Sciences, Vienna, Konrad-Lorenz-Straße, Tulln, Austria.
[3]Department of Crop Sciences, Institute of Agronomy, University of Natural Resources and Life Sciences, Vienna, Konrad-Lorenz-Straße, Tulln, Austria.

Corresponding author:
Jakob Santner (jakob.santner@boku.ac.at)

Email addresses of co-authors:
Stefan Wagner (stefan.wagner@unileoben.ac.at)
Christoph Hoefer (christoph.hoefer@gmail.com)
Thomas Prohaska (thomas.prohaska@unileoben.ac.at)

KEYWORDS:

chemical imaging, rhizosphere, diffusive gradients in thin films, laser ablation inductively coupled plasma mass spectrometry, trace element, plant nutrition

SUMMARY:

This protocol presents a workflow for sub-mm 2D visualization of multiple labile inorganic nutrient and contaminant solute species using diffusive gradients in thin films (DGT) combined with mass spectrometry imaging. Solute sampling and high-resolution chemical analysis are described in detail for quantitative mapping of solutes in the rhizosphere of terrestrial plants.

ABSTRACT:

We describe a method for two-dimensional (2D) visualization and quantification of the distribution of labile (i.e., reversibly adsorbed) inorganic nutrient (e.g., P, Fe, Mn) and contaminant (e.g., As, Cd, Pb) solute species in the soil adjacent to plant roots (the 'rhizosphere') at sub-millimeter (~100 µm) spatial resolution. The method combines sink-based solute sampling by the diffusive gradients in thin films (DGT) technique with spatially resolved chemical analysis by laser ablation inductively coupled plasma mass spectrometry (LA-ICP-MS). The DGT technique is based on thin hydrogels with homogeneously distributed analyte-selective binding phases. The variety of available binding phases allows for the preparation of different DGT gel types following simple gel fabrication procedures. For DGT gel deployment in the rhizosphere, plants are grown in flat, transparent growth containers (rhizotrons), which enable minimal invasive access to a soil-

grown root system. After a pre-growth period, DGT gels are applied to selected regions of interest for in situ solute sampling in the rhizosphere. Afterwards, DGT gels are retrieved and prepared for subsequent chemical analysis of the bound solutes using LA-ICP-MS line-scan imaging. Application of internal normalization using ^{13}C and external calibration using matrix-matched gel standards further allows for the quantification of the 2D solute fluxes. This method is unique in its capability to generate quantitative, sub-mm scale 2D images of multi-element solute fluxes in soil-plant environments, exceeding the achievable spatial resolution of other methods for measuring solute gradients in the rhizosphere substantially. We present the application and evaluation of the method for imaging multiple cationic and anionic solute species in the rhizosphere of terrestrial plants and highlight the possibility of combining this method with complementary solute imaging techniques.

INTRODUCTION

Nutrient acquisition by crop plants is a key factor in determining crop productivity. The processes governing efficient uptake of nutrients by crops have been studied intensely, especially the mechanisms controlling nutrient availability to and nutrient internalization by plant roots at the soil-root interface, the rhizosphere, are recognized for their role in crop nutrient acquisition. Important processes for plant nutrient uptake include: nutrient transport towards the root; dynamic sorption equilibria between species dissolved in the soil porewater and species bound to solid soil surfaces; microbial competition for nutrients; microbial mineralization of nutrients that are contained in soil organic matter; and nutrient internalization into the root symplasm. The uptake of inorganic trace metal(oid) contaminants is largely controlled by the same mechanisms.

Depending on nutrient and contaminant availability, plant demand and diffusivity in soil, differential nutrient patterns in the rhizosphere can be observed. For strongly sorbing elements with comparatively high internalization rates (e.g., P, Fe, Mn, Zn, As, Cd, Pb), depletion of the labile (i.e., reversibly adsorbed) element fraction compared to the bulk soil is found, with depletion zone widths often being ≤1 mm, while for more mobile nutrients such as NO_3^-, depletion zones can extend up to several centimeters[1]. Moreover, accumulation of elements such as Al and Cd has been observed when availability exceeds plant uptake rates[2,3].

Given the importance of rhizosphere processes in nutrient and contaminant cycling, several techniques for measuring the plant-available element fraction at high spatial resolution have been developed[4,5]. However, measuring small-scale labile solute distributions has proven to be challenging for several reasons. A major difficulty is to sample very small (low µL range) volumes of soil and/or porewater at defined positions adjacent to living plant roots to resolve the steep nutrient gradients in the rhizosphere. One approach to address this problem is to use micro-suction cups for the extraction of porewater samples[6]. With this method, A. Göttlein, A. Heim and E. Matzner [7] measured soil porewater nutrient concentrations in the vicinity of *Quercus robur* L. roots at a spatial resolution of ~1 cm. A difficulty of analyzing µL volumes of soil or soil solution is, that these small sample volumes, in combination with the low concentrations of all but the major nutrient species, require highly sensitive chemical analysis techniques.

An alternative system, capable of resolving nutrient gradients at a resolution down to ~0.5 mm, is to grow a root mat on the surface of a soil block, with a thin hydrophilic membrane layer separating soil from the roots[8,9]. In this configuration, solutes can pass through the membrane and roots can take up nutrients and contaminants from the soil while root exudates can diffuse into the soil. After the establishment of a dense root layer, the soil block can be sampled and sliced to obtained soil samples for subsequent extraction of element fractions. In this way, one-dimensional nutrient, and contaminant gradients, averaged across a relatively large area (~100 cm^2) can be analyzed.

A further challenge is to obtain samples of the labile, plant-available element fraction, since most chemical soil extraction techniques operate very differently compared to the mechanisms by which plants take up nutrients and contaminants. In many soil-extraction protocols, soil is mixed with an extractant solution with the aim to establish a (pseudo-)equilibrium between dissolved and sorbed element fraction. However, plants continuously internalize nutrients and, therefore, often progressively deplete the rhizosphere soil. Although equilibrium extraction protocols have been widely adopted as soil tests as they are easy to implement, the extracted nutrient fraction often does not represent the plant-available nutrient fraction well[10-13]. Sink methods which continuously deplete the sampled soil for nutrients have been proposed as advantageous methods and may better resemble the underlying nutrient uptake mechanism by mimicking the root uptake processes[10,11,14,15].

In addition to the methods described above, genuine imaging applications, capable of measuring continuous parameter maps with resolutions ≤100 µm across fields of view of several cm^2 have been developed for specific elements and soil (bio)chemical parameters[5]. Autoradiography can be used to image the element distribution in the rhizosphere provided that suitable radioisotopes are available[16]. Planar optodes enable visualization of important soil chemical parameters such as pH and pO_2[17-19], and enzyme activity or total protein distributions can be mapped using fluorescent indicator imaging techniques such as soil zymography[20-23] and/or root blotting methods[24]. While zymography and autoradiography are limited to the measurement of a single parameter at a time, pH and pO_2 imaging using planar optodes can be done concurrently. The more traditional root mat techniques provide 1D information only, while micro suction cups provide point measurements or low resolution 2D information, however both approaches allow for multi-element analysis. More recently, P. D. Ilhardt*,* et al.[25] presented a novel approach using laser induced breakdown spectroscopy (LIBS) to map 2D total multi-element distributions at a resolution of ~100 µm in soil-root core samples where the natural element distribution was preserved by careful sample preparation.

The only technique capable of targeted 2D sampling of multiple nutrient and contaminant solutes at high spatial resolution is the diffusive gradients in thin films (DGT) technique, a sink-based sampling method that immobilizes labile trace metal(loid) species in situ on a binding material embedded in a hydrogel layer[26,27]. DGT was introduced as a chemical speciation technique for measuring labile solutes in sediments and waters, and was soon adopted for its use in soils[28]. It enables sub-mm scale multi-element solute imaging, which was initially demonstrated in a river sediment[29], and has been developed further for its application in plant rhizospheres[30-33].

For DGT sampling, a gel sheet of a size of approximately 3 cm x 5 cm is applied onto a single plant root that is growing in the surface layer of a soil block, with a hydrophilic membrane separating the gel from the soil. During the contact time, labile nutrients and/or contaminants diffuse towards the gel and are bound immediately by the binding material incorporated in the gel. In this way, a concentration gradient, and thus a continuous net flux towards the gel is established and prevailed during the sampling time. After sampling, the hydrogel can be removed and analyzed using an analytical chemical technique allowing for spatially resolved analysis. A highly specialized and frequently used technique for this purpose is laser ablation inductively coupled plasma mass spectrometry (LA-ICP-MS). In some early studies, micro particle induced X-ray emission (PIXE) was also used[29]. DGT sampling combined with LA-ICP-MS analysis allows for multi-element chemical imaging at a spatial resolution of ~100 µm. If highly sensitive ICP-MS techniques (e.g., sector field ICP-MS) are employed, exceptionally low limits of detection can be achieved. In a study on the effect of liming on Zn and Cd uptake by maize[15], we were able to map labile Cd in the maize rhizosphere in uncontaminated soil with a limit of detection of 38 pg cm^{-2} of Cd per gel area. DGT, planar optodes, and zymography rely on diffusion of the target element from soil into a gel layer, which can be exploited for combined application of these methods in order to simultaneously, or consecutively, image a large number of parameters relevant for plant nutrient and contaminant uptake. Detailed information on analytical chemical aspects of DGT imaging, on the potential of combining DGT and other imaging methods, and on its applications is comprehensively reviewed in ref.[34,35].

In this article we describe how to carry out a solute imaging experiment using the DGT technique on roots of terrestrial plants in a unsaturated soil environment, including plant cultivation, gel fabrication, gel application, gel analysis and image generation. All steps are elaborated in detail, including notes on critical steps and experimental alternatives.

PROTOCOL

1. Fabrication of DGT gels

NOTE: Several DGT gel types are available for 2D imaging of labile solute species at high (sub-mm) spatial resolution[35]. Here, the fabrication of three well-characterized high resolution (HR)-DGT binding gels used in solute imaging applications is briefly summarized. Laboratory procedures for trace element analysis, as well as detailed fabrication procedures of all presented HR-DGT gels are described in the **Supporting Information (SI) sections S1 and S2**.

1.1. Polyurethane-based mixed anion and cation binding gel (HR-MBG; **SI S2.1**)[31]

1.1.1. Prepare a polyurethane gel suspension with homogeneously dispersed zirconium (IV) hydroxide and iminodiacetate (IDA) phases.

1.1.2. Coat the gel suspension in a thin film onto a glass plate and initiate gel formation by solvent evaporation to obtain a 0.1 mm-thin, tear-proof mixed anion and cation binding gel (HR-MBG).

1.2. Polyacrylamide-zirconia anion binding gel (HR-ABG; SI S2.2)[36]

1.2.1. Fabricate a 0.4 mm-thin agarose cross-linked polyacrylamide gel (APA) following established gel casting procedures[37] (**see SI S2.4** for a detailed protocol of the APA fabrication).

1.2.2. Precipitate zirconium (IV) hydroxide phases into the precast APA gel to obtain a 0.4 mm-thin anion binding gel (HR-ABG).

1.3. Polyacrylamide-iminodiacetate cation binding gel (HR-CBG; SI S2.3)[38]

1.3.1. Prepare a polyacrylamide gel suspension with homogeneously dispersed IDA phases.

1.3.2. Cast the gel between two glass plates and initiate the polymerization reaction to obtain a 0.4 mm-thin cation binding gel (HR-CBG) where the IDA phases are settled to one side of the gel.

2. Plant cultivation

NOTE: The experimental system uses rhizotrons[4] (**Figure 1**) to grow plants in unsaturated soil for solute imaging. First, rhizotron soil filling and watering are described, then details on the experimental plant growth are given. Details on the rhizotron design and soil substrate preparation before filling into the rhizotron are presented in the **SI section S3**.

[Place **Figure 1** here]

2.1. Rhizotron soil filling

2.1.1. Before filling the rhizotron with pre-moistened soil (gravimetric water content, w_{soil}, is known; see **SI S3.2**), close the watering holes at the back of the rhizotron using adhesive tape and remove the front plate and its fixation rails and screws.

2.1.2. Weigh the empty rhizotron (excluding the front plate, rails, and screws), eight 5 cm x 11 cm acrylic plates and 16 clamps (**Table of Materials**) and record the sum of weights.

2.1.3. Attach one small acrylic plate at the bottom of the rhizotron using two clamps on each side, with the pressure of the clamps directed onto the rhizotron frame, so the plate does not bend inwards and the volume is constant.

2.1.4. Incline the rhizotron slightly towards the small plastic plate and fill with pre-moistened soil up to a height of ~4 cm (**Figure 2A**). Distribute the soil inside the rhizotron by agitating the rhizotron slightly and gently compress the soil by a few mm (depending on the specific soil characteristics) with a compaction tool (**Figure 2B**).

2.1.5. Repeat 2.1.3 - 2.1.4 until the rhizotron is filled with soil (**Figure 2C**). Leave a gap of ~3 cm

at the top for the subsequent planting of seedlings into the rhizotron.

2.1.6. Weigh the soil-filled rhizotron (including 8 small plates and 16 clamps) and record the weight. From this, subtract the empty rhizotron weight obtained in 2.1.2 and record the weight difference, i.e., the mass of moist soil, $m_{\mathrm{m,soil\ rt}}$ (g), in the rhizotron.

2.1.7. Calculate the mass of dry soil in the rhizotron, $m_{\mathrm{d,soil\ rt}}$ (g), according to Eq. 1, and then calculate the dry soil bulk density, ρ_{d} (g cm^{-3}), in the rhizotron according to Eq. 2.

(Eq. 1) $m_{\mathrm{d,soil\ rt}} = m_{\mathrm{m,soil\ rt}} - m_{\mathrm{m,soil\ rt}} \times w_{\mathrm{soil}}$

(Eq. 2) $\rho_{\mathrm{d}} = \frac{m_{\mathrm{d,soil\ rt}}}{\mathrm{V_{rt}}}$

Here, V_{rt} (cm^3) is the total inner volume of the rhizotron.

NOTE: Typical ρ_{d} values in the rhizotron are between 1.0-1.4 g cm^{-3}. Do not exceed 1.5 g cm^{-3} as root growth might be impeded above this value.

2.1.8. Place the soil-filled rhizotron on a support box and remove all clamps and small plates from the rhizotron (**Figure 2D**). Carefully clean the rhizotron frame (i.e., edges) using tissue paper, as remaining soil particles on the frame can cause leaks.

NOTE: The exposed soil surface must be homogeneous and leveled with the rhizotron frame without any cracks or gaps. If not, empty the rhizotron and repeat 2.1.2 - 2.1.8.

2.1.9. Cut two pieces of polytetrafluoroethylene (PTFE) (**Table of Materials**) foil to 22 cm x 13 cm each. In addition, cut a piece of plastic foil to 46 cm x 15 cm. Record the sum of PTFE and plastic foil weights. Place the first piece of PTFE foil on the top half of the exposed soil surface in the rhizotron, extending ~1 cm over the soil level at the top of the rhizotron.

2.1.10. Carefully fix the PTFE foil to the rhizotron frame using adhesive tape (**Figure 2E**). Start by fixing one corner at the top of the rhizotron first, followed by its opposite corner and finally the two corners further down the rhizotron. Apply tension when fixing the corners 2-4 to ensure a flat foil surface. If folds emerge, open and re-fix the tape at individual corners (not all at once) until all folds are removed and the PTFE foil is flat and contiguous with the soil surface.

2.1.11. Place the second piece of PTFE foil on the lower end of the rhizotron, overlapping the upper PTFE foil piece by ~1 cm. Repeat 2.1.10 for fixing the second PTFE foil to the rhizotron.

2.1.12. Place the plastic foil (46 cm x 15 cm) onto the PTFE foils. Fix the plastic foil using the fixation procedure as detailed in 2.1.10.

2.1.13. Place a front plate onto the soil-filled and foil-covered rhizotron. Place one rail around

each side of the rhizotron and tighten the screws by hand to fix the rails and, thereby, the front plate to the rhizotron. The screws are positioned towards the closed side of the rhizotron, i.e., the side with the watering holes (**Figure 1A**).

[Place **Figure 2** here]

2.2. Watering the soil

2.2.1. Determine the water holding capacity (WHC) of the experimental soil in the rhizotron. To this end, manufacture two rhizotrons with an open bottom and fill them with soil as specified in section 2.1. Fully saturate these open, soil-filled rhizotrons by immersion in a water container for 16 h and drain the rhizotrons for 8 h.

2.2.2. Take a composite soil sample of ~50 g from random locations in the open-bottom rhizotrons and dry the sample at 105 °C to determine w_{soil} according to Eq. S1. The determined w_{soil} corresponds to the WHC of the soil and is, therefore, expressed as w_{WHC} (g g^{-1}).

2.2.3. Define the target w_{soil} in the experimental rhizotron. During the growth phase, set a w_{soil} of 60 % of the WHC (i.e., the WHC factor, f_{WHC} = 0.6) to supply plants with an adequate amount of water while avoiding anoxic conditions in the rhizotron.

2.2.4. Calculate the total mass of water to be added, $m_{\mathrm{w,add}}$ (g), to irrigate the soil in the rhizotron at the target w_{soil} according to Eq. 3. Account for the mass of water present in the soil in the rhizotron, $m_{\mathrm{w,soil\ rt}}$ (g).

(Eq. 3) $$m_{\mathrm{w,add}} = f_{\mathrm{WHC}} \times w_{\mathrm{WHC}} \times m_{\mathrm{d,soil\ rt}} - m_{\mathrm{w,soil\ rt}}$$

2.2.5. Divide $m_{\mathrm{w,add}}$ by the number of rhizotron watering holes (here 14) to obtain the mass of water to be added in each watering hole. Add water by pushing 10 mL pipette tips into the watering holes and letting the water flow into the soil by gravity (**Figure 3A**).

[Place **Figure 3** here]

2.3. Plant growth

2.3.1. Pre-germinate seeds of the experimental plant (e.g., on wet filter paper) according to the specific seed germination requirements until the radicle emerges (up to 1 cm long).

2.3.2. Plant up to two seedlings into the rhizotron as indicated in **Figure 3B**. At planting, add ~5 mL of water directly to the seedlings to support their growth. Cover the top opening of the rhizotron for the first ~two days after planting with a transparent, moisture-retaining film (**Table of Materials**). Wrap the rhizotron in aluminum foil to prevent microphytic growth.

NOTE: Apart from seedlings, plant cuttings can also be cultivated in rhizotrons.

2.3.3. Transfer the planted rhizotron into a growth room, with environmental conditions (i.e., temperature, humidity, light intensity) set to the specific plant requirements. Incline the rhizotron at 25°-35° to ensure root development alongside the front plate via gravitropism.

2.3.4. During plant growth, gravimetrically maintain the target water content in the rhizotron by periodical watering every 2-4 days using the rhizotron watering holes as detailed in 2.2.5. Keep the soil surface at the top opening moist by regular additions of ~5 mL water.

NOTE: If plants are grown for extended periods and the plant biomass is expected to substantially decrease the amount of water added to the rhizotron by the proposed method, account for the weight of the plant biomass by growing plants in separate rhizotron replicates and harvesting and weighing the plant tissues at defined intervals.

2.3.5. Once roots reach a suitable location along the front plate, preferentially in the center of the rhizotron, apply DGT gels for sampling the rhizospheric solute distribution.

3. Sampling the solute distribution

3.1. Gel application

3.1.1. Increase w_{soil} in the rhizotron from 60 % w_{WHC} to 80 % w_{WHC} 24 h before gel application as detailed in 2.2.4.-2.2.5. This ensures good soil-gel contact and allows solute diffusion into the gel while avoiding anoxic soil conditions during solute sampling.

3.1.2. Take a new, acid-cleaned front plate, align it on the rhizotron used for sampling, and mark the regions of interest (ROIs) on the plate. Transfer the plate into a laminar flow bench or any other dust- and metal-free environment, unmarked side facing up.

3.1.3. Cut the DGT binding gel on an acrylic support to the required rectangular size corresponding to the ROI, usually around 3 cm × 5 cm, using PTFE-coated razor blades. Cut the gel by pressing rather than sliding the razor blade to ensure a clear cut. Place the rectangular gel piece on the unmarked side of the plate at the marked location of the ROI.

NOTE: If HR-MBG is used, a 100 µm-thin spacer foil may be added underneath the gel to ensure that the gel is in good contact with the soil-root system.

3.1.4. Cut a 10 µm-thin polycarbonate membrane (0.2 µm pore size; **Table of Materials**) to a size which extends the gel size by ≥1 cm at each side and place the membrane onto the gel. Apply some water to remove air bubbles from the stack.

3.1.5. Fix the membrane along all four edges using vinyl electrical tape (**Table of Materials**). In the process, carefully remove air bubbles trapped in between the gel and the membrane using plastic tweezers. The tape must only get in contact with the membrane and not with the gel.

NOTE: If the tape comes in contact with the gel, air bubbles are trapped between the gel and the membrane, or the final membrane surface shows folds, the gel/membrane stack needs to be reassembled as the diffusive flux of solutes into the gel can be impaired[35] (repeat 3.1.3 - 3.1.5).

3.1.6. Place the rhizotron on a stand, remove the rails and carefully lift off the front plate (**Figure 3C**). Remove the plastic foil, cut off the PTFE foil at the edges of the rhizotron and slowly peel off the PTFE foil to avoid disturbance of the soil-root system (**Figure 3D**).

3.1.7. Take an orthogonal photo of the ROI using a digital single-lens reflex (DSLR) camera (**Table of Materials**) to facilitate the interpretation and presentation of the solute distribution based on the soil structure and root morphology (**Figure 3E**). Use a camera stand and, if available, a macro lens. Align the camera that the center of the photo corresponds to the center of the ROI, and the camera's focus plane is parallel to the soil surface. Include a scale bar (e.g., a ruler) in the photo.

3.1.8. Attach the plate equipped with the gel/membrane stack to the open rhizotron (**Figure 3F**). Therefore, align one edge of the plate with an edge of the rhizotron and gently 'bend' the plate towards the soil. This mode of application helps to avoid air bubbles between the gel/membrane stack and the soil-root system. Fix the front plate using the rails and screws.

NOTE: This step is critical and needs to be carried out carefully. The plate cannot be moved after establishing contact between the gel/membrane stack and the soil-root system without displacing soil and roots.

3.1.9. Record the exact starting time of gel deployment and take a photo of the deployed gel at the ROI as given in 3.1.7 (**Figure 3G**). Wrap the rhizotron in aluminum foil and transfer into the growth room until the end of the solute sampling period (often 24 h).

3.2. Gel retrieval

3.2.1. Place the rhizotron on a support box, carefully lift off the front plate and rinse the gel/membrane stack on the plate with water to wash off adhering particles (**Figure 4A**). Record the exact end time of gel deployment. Sample soil from the ROI to determine the actual w_{soil} in the rhizotron according to Eq. S1.

3.2.2. Transfer the front plate into the laminar flow bench, gel/membrane stack facing up. Retrieve the gel from the front plate by carefully removing first the tape along all four edges and then the polycarbonate membrane covering the gel (**Figure 4B**). Apply water to help the gel to float freely on a thin film of water on the plate with the soil-contact side facing up.

NOTE: It is critical to keep track of the gel orientation. The gel side exposed to the soil and roots must always face up (toward the user).

[Place **Figure 4** here]

3.3. Gel drying

3.3.1. Cut a rectangular piece of gel blotting paper (**Table of Materials**) and place a slightly smaller piece of a polyethersulfone membrane (0.45 µm pore size; **Table of Materials**) on top.

3.3.2. Transfer the gel from the plate onto the gel blotting paper/membrane stack using plastic tweezers, soil-contact side facing up. The gel must be relaxed (i.e., not stretched) and completely flat, without any air bubbles between gel and membrane. Apply some water onto the gel blotting paper/membrane stack to facilitate the gel transfer and positioning.

3.3.3. Cover the gel blotting paper/membrane/gel stack completely with a piece of plastic foil and label the gel sample and its orientation on the plastic foil (**Figure 4C**). Place the gel blotting paper/membrane/gel/plastic foil stack in a vacuum gel dryer (**Table of Materials**) and dry until the stack is fully desiccated (typically 48-72 h). For HR-MBG, set the temperature to 50-55 °C, for HR-ABG and HR-CBG best dry at room temperature.

3.3.4. Remove the gel blotting paper from the dried stack and transfer the gel, which is now inseparably merged with the polyethersulfone membrane, into a zip bag. The plastic foil cover stays on the gel until shortly before the LA-ICP-MS analysis.

3.3.5. Include a gel piece from the original gel sheet as a method blank, which does not get exposed to soil. Process the method blank gel identical to the sample gel following 3.3.2 - 3.3.4.

4. Chemical analysis of the DGT binding gel

NOTE: In this protocol, analysis of the solute distribution on the DGT binding gel is accomplished by LA-ICP-MS using a nanosecond 193 nm ArF excimer LA system equipped with a two-volume ablation cell coupled to a quadrupole ICP-MS (**Figure 5**). All instruments are listed in the **Table of Materials**. Alternatively, nanosecond 213 nm or 266 nm solid-state LA systems can be applied[36,39-43]. If enhanced sensitivity or mass resolution is required, sector field ICP-MS is an alternative to quadrupole ICP-MS[15,44]. Details on the preparation of DGT gel standards for external calibration and coupling of the LA system to the quadrupole ICP-MS are presented in the **SI sections S4 and S5**.

[Place **Figure 5** here]

4.1. Sample preparation for LA-ICP-MS

4.1.1. Transfer the dried gel samples, standards, and method blanks (which are merged with the polyethersulfone membrane support) onto individual pieces of double-sided adhesive tape (**Table of Materials**), gel side facing up. Crop excess tape parts to save space in the ablation cell.

4.1.2. Mount the dried gels onto glass plates. Use individual glass plates for each gel sample,

standard series, or method blank to allow for flexible arrangement on the LA sample stage (typical size of 10 cm × 10 cm). Use a glasscutter to adjust the glass plate size as needed. Fix the glass plates with the gels on the LA sample stage (**Figure 5B**) using plasticine (**Table of Materials**). Level the gel surface by adjusting the stage floor and lock the sample stage into the ablation cell.

4.2. LA-ICP-MS line-scan analysis

4.2.1. Couple the LA system to the ICP-MS as specified in the **SI section S5**. In the LA software (**Table of Materials**), set the camera light settings (i.e., '**Ring**', '**Coax**' and '**Transmitted**') to illuminate the gel surface in the ablation cell and focus onto the gel surface by adjusting the z-axis distance. Move to random locations across the cell to ensure that all gel surfaces are in focus.

4.2.2. Set the LA parameters in the '**Laser Setup**' window of the LA software. Typical settings used in LA-ICP-MS line-scan analysis of DGT gels are: mode continuous; energy output 20-30%; repetition rate 10-20 Hz; spot diameter 100-200 µm; scan speed 150-250 µm s^{-1}.

NOTE: The parameters need to be optimized for the type of gel used and may vary. Parameters can also be enhanced for increasing signal to noise ratio, spatial resolution, or reducing acquisition times depending on the experimental and instrumental setup. Use a relatively low energy output (≤40 %) and repetition rate (≤25 Hz) to avoid penetrating through the gels into the backing materials[39]. Make sure that the laser scan speed is ≤ the spot diameter divided by the total ICP-MS scan cycle duration (see 4.2.6) to avoid compression of the datapoints and thus a loss of resolution in scan direction[45]. For example, when setting a spot diameter of 200 µm and a total ICP-MS scan cycle duration of 0.25 s, the scan speed should be ≤800 µm s^{-1}.

4.2.3. Select the line tool and draw a single, ~1 mm-long line pattern across a gel standard. Right click the line pattern in the '**Scan Patterns**' window and verify that the LA parameters set in 4.2.3. have been adopted. Use the '**Duplicate Scans**' tool to duplicate this line four times, with a interline distance (distance between the line center) larger than the spot diameter (**Figure 6**). This approach offers a total of five parallel lines per gel standard (n = 5). Repeat this step for each gel standard, calibration blank and method blank.

4.2.4. Move to the gel sample and draw a single line along the top edge of the rectangular area to be analyzed. Duplicate the line to create parallel lines for the entire sample area as specified in 4.2.3. Use an interline distance of 300-400 µm. Make sure the focus (z-axis distance) is set correctly for each start and end point of each line.

NOTE: The spatial resolution of the analysis is higher along the scan direction compared to the interline distance. Therefore, start and end points of the lines may best follow the direction of the analyte gradients. For rhizosphere gradients, this is usually perpendicular to the root axis (**Figure 6)**.

[Place **Figure 6** here]

4.2.5. In the ICP-MS software (**Table of Materials**), set up a time-resolved '**Data Only**' method in the '**Method**' screen, select one or more suitable isotope(s) for every analyte and include ^{13}C as internal normalization standard[31,36,40-42]. Verify that detection of the isotopes is not impaired by interferences[46].

4.2.6. Set the total scan cycle duration of the ICP-MS method ('**Est. Reading Time**') to ≤0.5 s with appropriate dwell times per isotope (typically between 10-50 ms). Set the ICP-MS '**Readings**' to 1 and change the '**Readings/Replicate**' value to set the total measurement time per sample ('**Est. Sampling Time**'), i.e., per individual ablation line. This depends on the specific LA parameters and line distances set in 4.2.2 - 4.2.4.

4.2.7. For data reporting use an intensity versus time data collection mode and set the '**File Write Option**' to '**New Per Sample**' to create an individual data file (here .xl) for each ablation line.

4.2.8. Set up a '**Batch**' sample sequence in the ICP-MS '**Sample**' screen, with each sample entry corresponding to an individual ablation line set in 4.2.3 - 4.2.4.

4.2.9. Click '**Analyze Batch**' to initiate the sample sequence on the ICP-MS, which will wait with data acquisition until it is triggered by the first laser pulse (see **SI S5** for details on the trigger configuration).

4.2.10. In the LA software, select all lines to be analyzed and verify that the ICP-MS method ('**Est. Sampling Time**', see 4.2.6.) matches the duration of the individual line ablations, which is typically different for gel samples, standards and method blanks. Repeat 4.2.6. to adjust the ICP-MS method if necessary.

4.2.11. Click '**Emission**' in the '**Laser Energy**' window to recharge the laser head, and then click '**Run**' to open the '**Run Experiment**' window. Here, select '**Selected Patterns Only**', set the '**Washout Delay**' to 20-30 s, tick the '**Enable Laser During Scans**' box, and set the '**Laser Warmup Time**' to 10 s.

4.2.12. Click '**Run**' in the '**Run experiment**' window to start the line-scan analysis and monitor the raw signal intensity in counts per second (cps) for each isotope on the ICP-MS in real time. Each line should start ('**Laser Warmup Time**', 10 s) and end ('**Washout Delay**', 20-30 s) with a gas blank.

4.2.13. Monitor the laser fluence (J cm^{-2}) during analysis to assess the laser stability. If the fluence varies largely, abort the analysis, and verify that the laser source and/or its mirror system are fully functional.

4.2.14. After the analysis, stop the ICP-MS plasma and set the carrier gas flow rate on the LA system to 0 mL min^{-1}. Remove the gels from the ablation cell and store in zip bags for further use.

4.3. Data processing and calibration

4.3.1. Import the raw data file (.xl) for each ablated line in spreadsheet software (**Table of Materials**). The raw data table shows the ICP-MS readings (datapoints) for each isotope in cps and the corresponding time points in s. List all lines next to each other in different columns.

4.3.2. Evaluate the line-scan data for signal stability of the internal standard (^{13}C) and adequate washout times.

4.3.3. Calculate an average gas blank for each isotope from all gas blank values recorded before the line ablations (i.e., during the laser warm-up time) and subtract the average gas blank from the corresponding raw intensities for each isotope to correct for the background signal.

4.3.4. Apply internal normalization by dividing the signal intensity of each isotope (cps) by the signal intensity of the internal standard (cps) for each datapoint to correct for variations in the amount of material ablated and instrumental drift.

4.3.5. Crop data before the start and after the end of each ablated line to remove the background signal. Transpose the data table to obtain a grid matrix where each row corresponds to an ablated line and each column to a normalized isotope intensity value. Separate the matrices for each isotope into individual worksheets.

4.3.6. Calculate the average normalized signal intensity ratio per isotope for the calibration standards and calibration blank and compute the calibration function ($y = ax + b$) using a linear regression model with the gel standard analyte loadings (µg cm^{-2}; see **SI S4**) as x-values. Evaluate the calibration function of each isotope for linearity[47].

4.3.7. Apply the calibration function to the sample data matrix. Convert the normalized signal intensity ratios, I_{norm}, to gel analyte loadings, Γ_{DGT} (µg cm^{-2}), and subsequently to time-averaged solute fluxes, f_{DGT} (pg cm^{-2} s^{-1}), for each isotope and datapoint according to Eq. 4 and Eq. 5:

(Eq. 4) $$\Gamma_{\mathrm{DGT}} = \frac{I_{\mathrm{norm}} - b}{a}$$

(Eq. 5) $$f_{\mathrm{DGT}} = \frac{\Gamma_{\mathrm{DGT}}}{t} \times 10^{6}$$

Here, a is the slope of the calibration line, b is the intercept of the calibration line, and t (s) is the gel deployment time during solute sampling.

4.3.8. Save the calibrated sample data matrix for each analyte as txt-file.

4.4. Image generation

NOTE: Make sure to avoid any pixel interpolation operation during all steps of image generation,

as this may lead to artificially smoothed solute flux gradients in the resulting images.

4.4.1. Import the calibrated sample data matrix (.txt) as text image in the image analysis software (**Table of Materials**).

4.4.2. Calculate the distance per pixel in x-direction (i.e., lateral resolution) by multiplying the laser scan speed with the total ICP-MS scan cycle duration (e.g., assuming a scan speed of 200 µm s^{-1} and a total scan cycle duration of 0.25 s the lateral resolution equates to 50 µm). The distance per pixel in y-direction equates to the interline distance (**Figure 6**).

4.4.3. Calculate the aspect ratio correction factor of the image. Therefore, divide the distance per pixel in y-direction (e.g., 300 µm) by the distance per pixel in x-direction (e.g., 50 µm). Apply the obtained y/x correction factor (in this example 6) under '**Scale**'. Apply the distance per pixel (in µm or mm) in x-direction as scaling under '**Set scale**'.

4.4.4. Apply a '**Look Up Table**' i.e., pseudo-color scale for better visualization of chemical gradients in the solute image and adjust the image 'color balance' to control the lower/upper limits of the display range. Add a '**Calibration bar**' and save the solute image as tiff-file.

4.4.5. Copy the solute image using the '**Copy to System**' command in the image analysis software and paste into desktop publishing software (**Table of Materials**). Scale-match, align and compose the solute image with the photo of the ROI obtained in 3.1.7.

NOTE: Before copying, resize the solute image by e.g., factor 10 via applying a '**X Scale**' of 10 and a '**Y Scale**' of 10 under '**Set scale**' to ensure sufficient pixels for high-resolution publishing.

REPRESENTATIVE RESULTS

To demonstrate the capability and data detail of the DGT imaging method, we compiled the sub-mm, 2D flux distribution of multiple labile nutrient and contaminant solute species in soil adjacent to roots of *Fagopyrum esculentum* and *Salix smithiana* (**Figure 7**). Approximate times for general procedural steps of the protocol are presented in **Table 1**.

[Place **Table 1** here]

Solute images in **Figure 7** were generated in three different studies using either HR-MBG or HR-CBG binding gels. The chemical images show the 2D solute flux distribution at a spatial resolution of 82-120 µm along the x-axis and 300-400 µm along the y-axis, depending on the LA-ICP-MS parameters used. Because no interpolation was applied during image calibration and resizing, single pixels represent measured datapoints. Alignment of the solute images with a photographic image of the ROI reveals that the sub-mm, 2D solute flux distribution of different elements is highly variable according to soil structure and root morphology. This can be attributed to the differential biogeochemical behavior of the elements in the soil-rhizosphere-plant system, and their interaction with the soil matrix and the plant roots.

In **Figure 7A** labile inorganic Mg, Al, P, Mn and Fe solute fluxes were visualized around a young *F. esculentum* root grown in carbonate-free soil fertilized with NH_4NO_3. The sub-mm solute distribution showed zones of decreased Al, P and Fe fluxes alongside older root sections due to root uptake, and highly increased Mg, Al, P, Mn and Fe fluxes at the root apex due to localized P mobilization processes of the *F. esculentum* root. Note that the root tip is located somewhat behind the soil surface and therefore hardly visible in the photographic image. **Figure 7B** shows the distribution of labile trace metals, including Mn, Fe, Zn, Cd and Pb around a root of metal-tolerant *S. smithiana* grown in a soil moderately contaminated with Zn, Cd and Pb. The solute images visualized distinct depletion particularly of Zn, Cd and Pb at the immediate root position, showing that *S. smithiana* roots act as a localized sink for labile trace metals in contaminated soil. Besides, localized Zn, Cd and Pb flux increases can be observed, indicating accumulation of these trace metals at the immediate soil-root interface.

In addition to multi-elemental solute imaging, the presented method can also be combined with complementary diffusion-based imaging techniques such as planar optodes[34]. This is demonstrated in **Figure 7C**, where the distribution of labile trace metals in the rhizosphere of *S. smithiana* was co-localized with the distribution of pH using a combined, single-layer planar optode-DGT cation binding gel[33]. The soil substrate was fertilized with $(NH_4)_2SO_4$, leading to a pH decrease along the root axes by ~1 unit as compared to bulk soil. The pH decreases were co-localized with increased solute fluxes of Mn, Fe, Co, Ni, Cu and Pb, suggesting pH-induced metal solubilization.

Moreover, these example results show some of the potential imaging artefacts that may be obtained. For example, structural soil inhomogeneities, e.g., observed as a horizontal line in the lower third of the ROI image of **Figure 7A**, can cause soil-gel contact discontinuities resulting in limited diffusion at this location into the binding gel. Conversely, excessive soil compaction in the rhizotron can lead to poor porosity resulting in an artificial shift of the soil redox status towards anoxia. This is illustrated in **Figure 7B**, where extensive areas of highly elevated Mn and Fe fluxes in the solute images visually matched with a dense layer of soil in the ROI image. This suggests a decreased soil redox potential due to high soil compaction, resulting in reductive dissolution and solubilization of the highly redox-sensitive elements. Careful rhizotron filling and visual inspection of the soil surface directly after filling is therefore recommended.

[Place **Figure 7** here]

FIGURE AND TABLE LEGENDS

Figure 1: Rhizotron design (not to scale). (**A**) Exploded view of a rhizotron growth container. (**B**) Assembled rhizotron during plant growth.

Figure 2: Rhizotron assembly and filling to grow plants in soil for solute imaging in the rhizosphere. (**A**) Soil filling into the rhizotron. (**B**) Compaction of the filled soil using a compaction tool. (**C**) Soil-filled rhizotron with small acrylic plates and clamps. (**D**) Soil-filled rhizotron with exposed soil surface. (**E**) Soil-filled rhizotron partly covered with a protective PTFE foil.

Figure 3: Rhizotron handling and DGT gel application. (**A**) Soil watering using 10 mL pipette tips in the watering holes in the back of the rhizotron. (**B**) Planting of seedlings (indicated as green spots) into the soil-filled and closed rhizotron. (**C**) Rhizotron planted with *Salix smithiana* cuttings and removed front plate and plastic foil cover. (**D**) Carefully peeling off the PTFE foil cover before DGT gel application. (**E**) High-resolution photo of the soil-root interface ROI. (**F**) Application of the front plate equipped with the DGT gel onto the rhizotron. (**G**) Photo of the ROI with the DGT gel applied during solute sampling.

Figure 4: DGT gel retrieval and preparation for drying upon solute sampling. (**A**) Plate with the DGT gel and rhizotron directly after solute sampling. (**B**) Retrieval of the DGT gel from the plate in a laminar flow bench. (**C**) Stack of gel blotting paper/polyethersulfone membrane/DGT gel/plastic foil cover for gel drying. Note that the gel is slightly colored after its deployment on the rhizosphere soil.

Figure 5: LA-ICP-MS setup for DGT gel analysis. (**A**) Nanosecond 193 nm ArF excimer LA system and quadrupole ICP-MS. (**B**) Dried gels mounted onto glass plates and fixed on the LA sample stage ready for introduction into the ablation cell. (**C**) Nebulizer gas (Ar) from ICP-MS and aerosol carrier gas (He or Ar) from ablation cell connected to the ICP via a two-way Y-splitter and torch adapter fitting.

Figure 6: Schematic of the DGT LA-ICP-MS experimental design (not to scale). The illustration depicts the DGT-based in situ solute sampling in the rhizosphere and the LA-ICP-MS mapping of the solute distribution on the gel surface, including a close-up showing exemplary line-scan dimensions and parameters. Note that the DGT gel is horizontally flipped when transferred from the rhizosphere soil onto the glass plate, as indicated by the position of the rectangle at the bottom corner of the DGT gel.

Figure 7: Sub-mm 2D distribution of labile nutrient and contaminant solute species across different soil-root interfaces. (**A**) Distribution of anionic P and cationic Mg, Al, Mn, and Fe solutes around a young *F. esculentum* root. Co-localized sampling of anionic and cationic solutes was achieved using HR-MBG for 24 h at a soil water saturation of ~75% WHC. The Al, P and Mn images are displayed as calibrated f_{DGT} values (pg cm^{-2} s^{-1}), whereas Mg and Fe images show ^{13}C-normalized intensities. Scale bar represents 1 cm. This figure is adapted from ref.[48]. (**B**) Distribution of Mn, Fe, Zn, Cd and Pb around a *S. smithiana* root grown in soil moderately contaminated with Zn, Cd and Pb. Cationic trace metal solutes were sampled using HR-CBG for 20 h at a soil water saturation of ~80 % WHC. All images are displayed as calibrated f_{DGT} values (pg cm^{-2} s^{-1}). Scale bar represents 0.5 cm. This figure is adapted from ref.[3]. (**C**) Distribution of pH and multiple cationic solutes around *S. smithiana* roots grown in soil spiked with Cd. Co-localization of pH and solute dynamics was achieved using a modification of the HR-MBG protocol, allowing for simultaneous solute sampling and planar optode imaging[33]. The Mn, Cu, Zn and Cd images are displayed as calibrated f_{DGT} values (pg cm^{-2} s^{-1}), whereas Fe, Co, Ni and Pb images show ^{13}C-normalized intensities. Scale bar represents 1 cm. This figure is adapted from ref.[33]. The presented figures are reproduced from the cited articles[3,33,48] licensed under CC BY.

Table 1: Approximate times for general steps of the DGT LA-ICP-MS technique.

DISCUSSION

The solute imaging protocol presented here is a versatile method to visualize and quantify 2D nutrient and contaminant fluxes in soil-plant environments. It is unique in its capability to generate sub-mm scale multi-element images of labile solute species at the soil-root interface, exceeding the achievable spatial resolution of alternative methods for measuring solute gradients in the rhizosphere substantially[4]. The targeted in situ sampling approach of DGT, in combination with a highly sensitive chemical analysis method such as LA-ICP-MS, facilitates the detailed investigation of solute flux dynamics around individual plant roots grown in soil or similar substrates. Due to the sink-based sampling process, the obtained images reflect the lability of the visualized solutes, and therefore are an estimation of their plant-availability[10]. Although the method-inherent measurement of solute fluxes bears considerable advantages like the interpretability as plant-available nutrient fractions, flux measurements are much less straight-forward to understand than porewater concentration measurements. The standard DGT sampling geometry in bulk soil applications (specifically the 0.8 mm-thick diffusion gels used in that setup) allows for comparing the actual porewater concentration, c_{soln}, and a time-averaged porewater concentration estimate by a bulk DGT measurement, c_{DGT}, and for the interpretation of these parameters regarding the resupply dynamics of a solute species. However, such comparison cannot be done based on imaging DGT application with very thin diffusion layers, as the derived c_{DGT} values are unrealistically small[34]. DGT imaging results are therefore not always simple and quick to interpret and are often not directly comparable to more conventional porewater concentration measurements.

When applying the method, a few critical steps need to be carefully considered, mainly related to filling and watering the rhizotron growth containers. During filling the soil into the rhizotron, it is very important to avoid compacting the soil too much, as the plant roots cannot penetrate strongly compacted soil and root growth will be inhibited. We have observed roots avoiding strongly compacted soil and growing along the inner edges of the rhizotron growth container, where the soil is usually less compacted. In this case, individual roots located in the center of the rhizotrons, where DGT gels can be applied conveniently, may not develop at all, effectively inhibiting successful gel application. In our laboratory, experience showed that dry soil bulk densities of 1.0-1.4 g cm^{-3} allow unimpeded root development. Moreover, excessive soil compaction is also a potential source of artefacts regarding the solubility of redox-sensitive elements and biogeochemically associated species. As the total pore volume is reduced and the pore diameter distribution is shifted towards lower diameters in highly compacted soil, less air-filled larger-diameter pore volume is available, which may lead to reductive conditions locally. Consequently, $Mn^{III/IV}$- and Fe^{III}-oxides may be reduced, leading to increased Mn^{2+} and Fe^{2+} fluxes. The dissolution of Fe-oxides, which are important sorption sites e.g., for phosphate and micronutrients, may liberate sorbed and/or co-precipitated species and thereby cause artificially elevated fluxes of the biogeochemically associated species. A similar issue may arise if the growth containers are watered too much. Evaporation via the small soil surface area at the top of the growth container is low and the soil may remain water-saturated for up to several weeks after

planting, which may also cause redox artefacts.

Another important consideration is the chemical functionality of the fabricated HR-DGT binding gel. By following the protocol, thin gels with a homogeneous distribution of binding phases are obtained. If the gels have areas of inhomogeneous material distribution (e.g., holes in the gel or aggregates of binding phases) these areas need to be removed or, if too extensive, the gel fabrication protocol needs to be repeated. If prepared correctly, the gel must be able to bind the target solute species that diffuse into the gel immediately and quantitatively[27], which is determined by the analyte-specific gel binding capacity. While exceeding the gel capacity is less problematic in uncontaminated soils, it should be considered in metal-contaminated soils and saline soil environments. Saturation of the gel binding phases will not only impair quantitative solute sampling, but also result in lateral diffusion of solutes between binding phases in the gel, leading to an indefinite localization of small-scale solute flux features. Thus, if very high quantities of labile nutrient/contaminant species are expected in the target soil environment, preliminary tests should be performed. For estimating expected DGT loadings, bulk soil DGT piston sampling followed by gel elution and wet-chemical analysis can be applied[15,49]. If necessary, DGT deployment times may be adjusted to reduce the gel contact time and thus avoid gel saturation above capacity thresholds. Conversely, preliminary tests can also be helpful to identify required gel contact times and/or LA-ICP-MS sensitivities if very low solute loadings are expected, which may be important for mapping trace element solutes at natural soil background levels[15]. Besides, correct DGT gel functioning should be verified before its experimental application via controlled loading of gels in the preparation of DGT LA-ICP-MS calibration standards. The gel standard provides a matrix-matched reference gel analyte loading that can be used to assess if the sample gel loading determined by LA-ICP-MS is within the expected range. If unable to obtain a signal which is different from the gas and method blank background noise, the operator must ensure that laboratory procedures for trace element analysis were implemented and all protocol steps were performed correctly. Sometimes, the DGT gel is accidentally flipped after solute sampling with the soil-exposed, loaded side facing towards the glass plate rather than the laser beam, resulting in low signal intensities and erroneously flipped features in the final solute flux images.

During the LA-ICP-MS analysis, a large quantity of data is generated, which takes considerable time to evaluate. In our lab, we use in-house data evaluation scripts tailored for our target data output format using standard spreadsheet software. After semi-automated sorting and calibration, image plotting is conducted using open source, open access image analysis tools (ImageJ, Fiji[50]). This approach allows full control over data sorting, evaluation, and presentation, which is essential because the collected data correspond to rectangular, and not quadratic pixels, which needs to be properly displayed in the generated solute maps. Moreover, during data processing, any pixel interpolation should be carefully avoided. Pixel interpolation leads to smoothed gradients in the chemical images, resulting in softened, often circular element distribution features and is therefore an undesirable alteration of the original data. Pixel interpolation is a standard procedure in re-scaling and re-formatting operations in many image processing software products but can be deselected usually.

In conclusion, the described method is a significant advancement for understanding nutrient and

contaminant dynamics in natural soil-rhizosphere-plant systems. In addition to DGT-only applications, the method can be combined with other, diffusion-based imaging techniques like planar optodes[3,33,42,43,48,51] and zymography[20-24], and may be developed further for including additional elements and soil parameters.

ACKNOWLEDGMENTS:

This study was co-funded by the Austrian Science Fund (FWF): P30085-N28 (Thomas Prohaska) and the Austrian Science Fund (FWF) and the Federal State of Lower Austria: P27571-BBL (Jakob Santner).

DISCLOSURES:

The authors have nothing to disclose.

REFERENCES

1. Hinsinger, P., Gobran, G. R., Gregory, P. J., Wenzel, W. W. Rhizosphere geometry and heterogeneity arising from root-mediated physical and chemical processes. *New Phytologist.* **168** (2), 293-303 (2005).
2. Jungk, A. in *Plant Roots: The Hidden Half.* Marcel Dekker, New York. ch35, 587-616 (2002).
3. Hoefer, C., Santner, J., Puschenreiter, M., Wenzel, W. W. Localized metal solubilization in the rhizosphere of Salix smithiana upon sulfur application. *Environmental Science & Technology.* **49** (7), 4522-4529 (2015).
4. Luster, J., Göttlein, A., Nowack, B., Sarret, G. Sampling, defining, characterising and modeling the rhizosphere—the soil science tool box. *Plant and Soil.* **321** (1), 457-482 (2009).
5. Oburger, E., Schmidt, H. New Methods To Unravel Rhizosphere Processes. *Trends in Plant Science.* **21** (3), 243-255 (2016).
6. Göttlein, A., Hell, U., Blasek, R. A system for microscale tensiometry and lysimetry. *Geoderma.* **69** (1), 147-156 (1996).
7. Göttlein, A., Heim, A., Matzner, E. Mobilization of aluminium in the rhizosphere soil solution of growing tree roots in an acidic soil. *Plant and Soil.* **211** (1), 41-49 (1999).
8. Hinsinger, P., Gilkes, R. J. Dissolution of phosphate rock in the rhizosphere of five plant species grown in an acid, P-fixing mineral substrate. *Geoderma.* **75** (3), 231-249 (1997).
9. Wenzel, W. W., Wieshammer, G., Fitz, W. J., Puschenreiter, M. Novel rhizobox design to assess rhizosphere characteristics at high spatial resolution. *Plant and Soil.* **237** (1), 37-45 (2001).
10. Degryse, F., Smolders, E., Zhang, H., Davison, W. Predicting availability of mineral elements to plants with the DGT technique: a review of experimental data and interpretation by modelling. *Environmental Chemistry.* **6** (3), 198-218 (2009).
11. Mason, S., McNeill, A., McLaughlin, M. J., Zhang, H. Prediction of wheat response to an application of phosphorus under field conditions using diffusive gradients in thin-films (DGT) and extraction methods. *Plant and Soil.* **337** (1), 243-258 (2010).
12. Six, L., Smolders, E., Merckx, R. The performance of DGT versus conventional soil phosphorus tests in tropical soils—maize and rice responses to P application. *Plant and Soil.* **366** (1), 49-66 (2013).
13. Mason, S. D., McLaughlin, M. J., Johnston, C., McNeill, A. Soil test measures of available P

(Colwell, resin and DGT) compared with plant P uptake using isotope dilution. *Plant and Soil.* **373** (1), 711-722 (2013).
14. Freese, D., Lookman, R., Merckx, R., van Riemsdijk, W. H. New Method for Assessment of Long-Term Phosphate Desorption from Soils. *Soil Science Society of America Journal.* **59** (5), 1295-1300 (1995).
15. Smolders, E., Wagner, S., Prohaska, T., Irrgeher, J., Santner, J. Sub-millimeter distribution of labile trace element fluxes in the rhizosphere explains differential effects of soil liming on cadmium and zinc uptake in maize. *Science of The Total Environment.* **738**, 140311 (2020).
16. Bhat, K. K. S., Nye, P. H. Diffusion of phosphate to plant roots in soil. *Plant and Soil.* **38** (1), 161-175 (1973).
17. Glud, R. N., Ramsing, N. B., Gundersen, J. K., Klimant, I. Planar optrodes: a new tool for fine scale measurements of two-dimensional O2 distribution in benthic communities. *Marine Ecology Progress Series.* **140**, 217-226 (1996).
18. Blossfeld, S., Gansert, D. A novel non-invasive optical method for quantitative visualization of pH dynamics in the rhizosphere of plants. *Plant, Cell & Environment.* **30** (2), 176-186 (2007).
19. Larsen, M., Borisov, S. M., Grunwald, B., Klimant, I., Glud, R. N. A simple and inexpensive high resolution color ratiometric planar optode imaging approach: application to oxygen and pH sensing. *Limnology and Oceanography: Methods.* **9** (9), 348-360 (2011).
20. Spohn, M., Carminati, A., Kuzyakov, Y. Soil zymography – A novel in situ method for mapping distribution of enzyme activity in soil. *Soil Biology and Biochemistry.* **58**, 275-280 (2013).
21. Spohn, M., Kuzyakov, Y. Spatial and temporal dynamics of hotspots of enzyme activity in soil as affected by living and dead roots—a soil zymography analysis. *Plant and Soil.* **379** (1), 67-77 (2014).
22. Heitkötter, J., Marschner, B. Soil zymography as a powerful tool for exploring hotspots and substrate limitation in undisturbed subsoil. *Soil Biology and Biochemistry.* **124**, 210-217 (2018).
23. Guber, A. K., Kravchenko, A. N., Razavi, B. S., Blagodatskaya, E., Kuzyakov, Y. Calibration of 2-D soil zymography for correct analysis of enzyme distribution. *European Journal of Soil Science.* **70** (4), 715-726 (2019).
24. Lin, V. S. et al. Non-destructive spatial analysis of phosphatase activity and total protein distribution in the rhizosphere using a root blotting method. *Soil Biology and Biochemistry.* **146** 107820 (2020).
25. Ilhardt, P. D. et al. High-resolution elemental mapping of the root-rhizosphere-soil continuum using laser-induced breakdown spectroscopy (LIBS). *Soil Biology and Biochemistry.* **131**, 119-132 (2019).
26. Davison, W., Zhang, H. In situ speciation measurements of trace components in natural waters using thin-film gels. *Nature.* **367** (6463), 546-548 (1994).
27. Davison, W. *Diffusive Gradients in Thin-Films for Environmental Measurements*. Cambridge University Press, 2016.
28. Zhang, H., Davison, W., Knight, B., McGrath, S. In Situ Measurements of Solution Concentrations and Fluxes of Trace Metals in Soils Using DGT. *Environmental Science & Technology.* **32** (5), 704-710 (1998).
29. Davison, W., Fones, G. R., Grime, G. W. Dissolved metals in surface sediment and a

878 microbial mat at 100-µm resolution. *Nature.* **387** (6636), 885-888 (1997).
879 30. Santner, J. et al. High-resolution chemical imaging of labile phosphorus in the rhizosphere
880 of Brassica napus L. cultivars. *Environmental and Experimental Botany.* **77**, 219-226 (2012).
881 31. Kreuzeder, A., Santner, J., Prohaska, T., Wenzel, W. W. Gel for simultaneous chemical
882 imaging of anionic and cationic solutes using diffusive gradients in thin films. *Analytical*
883 *Chemistry.* **85** (24), 12028-12036 (2013).
884 32. Kreuzeder, A., Santner, J., Zhang, H., Prohaska, T., Wenzel, W. W. Uncertainty evaluation
885 of the diffusive gradients in thin films technique. *Environmental Science and Technology.* **49** (3),
886 1594-1602 (2015).
887 33. Hoefer, C., Santner, J., Borisov, S. M., Wenzel, W. W., Puschenreiter, M. Integrating
888 chemical imaging of cationic trace metal solutes and pH into a single hydrogel layer. *Analytica*
889 *Chimica Acta.* **950**, 88-97 (2017).
890 34. Santner, J., Larsen, M., Kreuzeder, A., Glud, R. N. Two decades of chemical imaging of
891 solutes in sediments and soils--a review. *Analytica Chimica Acta.* **878**, 9-42 (2015).
892 35. Santner, J., Williams, P. N. in *Diffusive Gradients In Thin-Films For Environmental*
893 *Measurements*. ed W. Davison. Cambridge University Press. Ch. 8, 174-215, (2016).
894 36. Guan, D.-X. et al. Novel Precipitated Zirconia-Based DGT Technique for High-Resolution
895 Imaging of Oxyanions in Waters and Sediments. *Environmental Science & Technology.* **49** (6),
896 3653-3661 (2015).
897 37. Zhang, H., Davison, W. Performance Characteristics of Diffusion Gradients in Thin Films
898 for the in Situ Measurement of Trace Metals in Aqueous Solution. *Analytical Chemistry.* **67** (19),
899 3391-3400 (1995).
900 38. Warnken, K. W., Zhang, H., Davison, W. Performance characteristics of suspended
901 particulate reagent-iminodiacetate as a binding agent for diffusive gradients in thin films.
902 *Analytica Chimica Acta.* **508** (1), 41-51 (2004).
903 39. Warnken, K. W., Zhang, H., Davison, W. Analysis of Polyacrylamide Gels for Trace Metals
904 Using Diffusive Gradients in Thin Films and Laser Ablation Inductively Coupled Plasma Mass
905 Spectrometry. *Analytical Chemistry.* **76** (20), 6077-6084 (2004).
906 40. Gao, Y., Lehto, N. A simple laser ablation ICPMS method for the determination of trace
907 metals in a resin gel. *Talanta.* **92** (Supplement C), 78-83 (2012).
908 41. Lehto, N. J., Davison, W., Zhang, H. The use of ultra-thin diffusive gradients in thin-films
909 (DGT) devices for the analysis of trace metal dynamics in soils and sediments: a measurement
910 and modelling approach. *Environmental Chemistry.* **9** (4), 415-423 (2012).
911 42. Williams, P. N. et al. Localized flux maxima of arsenic, lead, and iron around root apices in
912 flooded lowland rice. *Environmental Science & Technology.* **48** (15), 8498-8506 (2014).
913 43. Lehto, N. J., Larsen, M., Zhang, H., Glud, R. N., Davison, W. A mesocosm study of oxygen
914 and trace metal dynamics in sediment microniches of reactive organic material. *Scientific*
915 *Reports.* **7** (1), 11369 (2017).
916 44. Zitek, A., Aléon, J., Prohaska, T. in *Sector Field Mass Spectrometry for Elemental and*
917 *Isotopic Analysis.* The Royal Society of Chemistry. 152-182 (2015).
918 45. Lear, J., Hare, D., Adlard, P., Finkelstein, D., Doble, P. Improving acquisition times of
919 elemental bio-imaging for quadrupole-based LA-ICP-MS. *Journal of Analytical Atomic*
920 *Spectrometry.* **27** (1), 159-164 (2012).
921 46. May, T. W., Wiedmeyer, R. H. A table of polyatomic interferences in ICP-MS. *Atomic*

Spectroscopy. **19** (5), 150-155 (1998).
47. Raposo, F. Evaluation of analytical calibration based on least-squares linear regression for instrumental techniques: A tutorial review. *TrAC Trends in Analytical Chemistry.* **77**, 167-185 (2016).
48. Kreuzeder, A. et al. In situ observation of localized, sub-mm scale changes of phosphorus biogeochemistry in the rhizosphere. *Plant and Soil.* **424** (1) 573-589 (2018).
49. Hooda, P. S., Zhang, H., Davison, W., Edwards, A. C. Measuring bioavailable trace metals by diffusive gradients in thin films (DGT): soil moisture effects on its performance in soils. *European Journal of Soil Science.* **50** (2), 285-294 (1999).
50. Schindelin, J. et al. Fiji: an open-source platform for biological-image analysis. *Nature Methods.* **9** (7), 676-682 (2012).
51. Wagner, S. et al*.* Arsenic redox transformations and cycling in the rhizosphere of Pteris vittata and Pteris quadriaurita. *Environmental and Experimental Botany.* **177**, 104122 (2020).

Figure 1

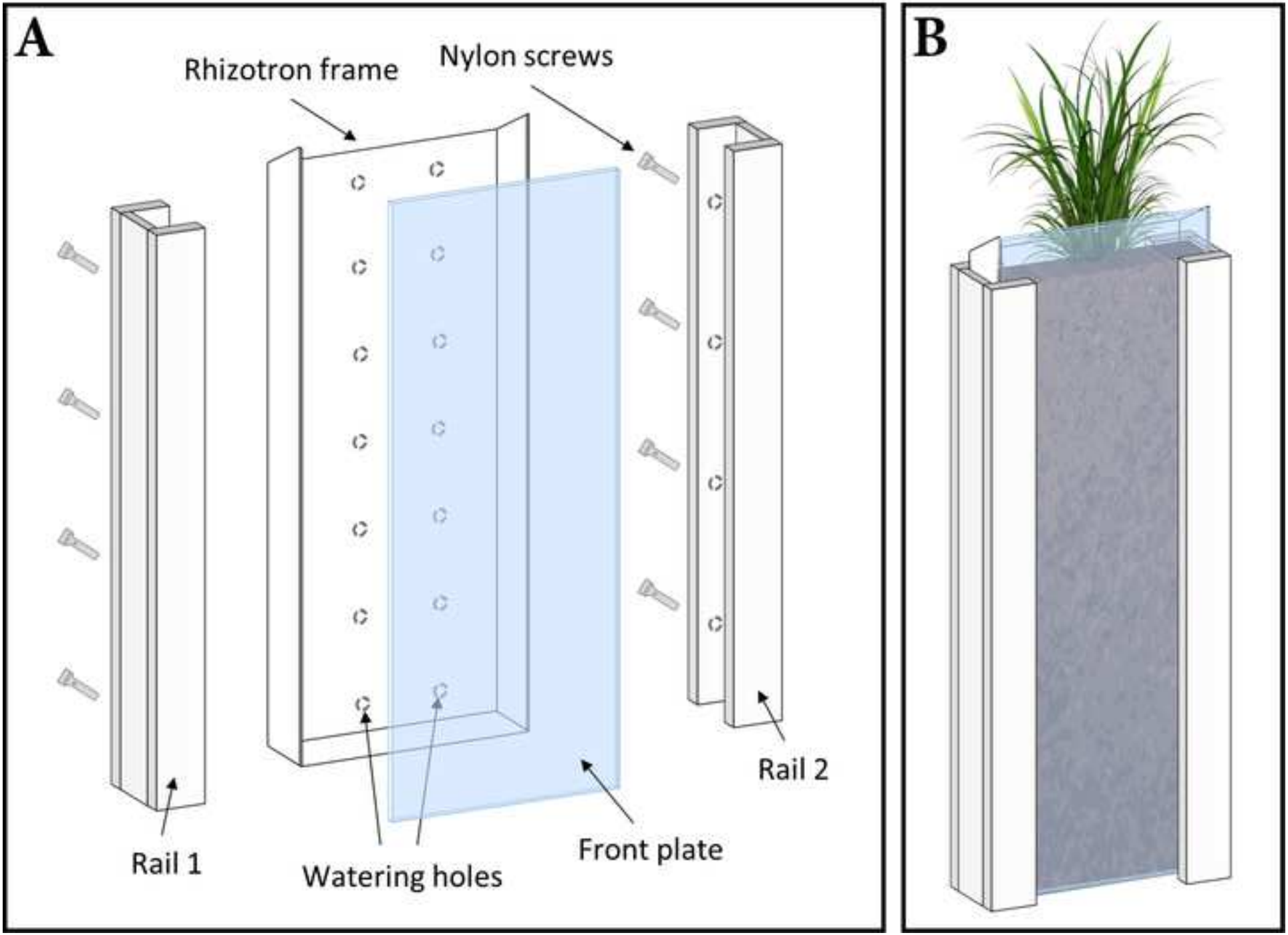

Figure 2

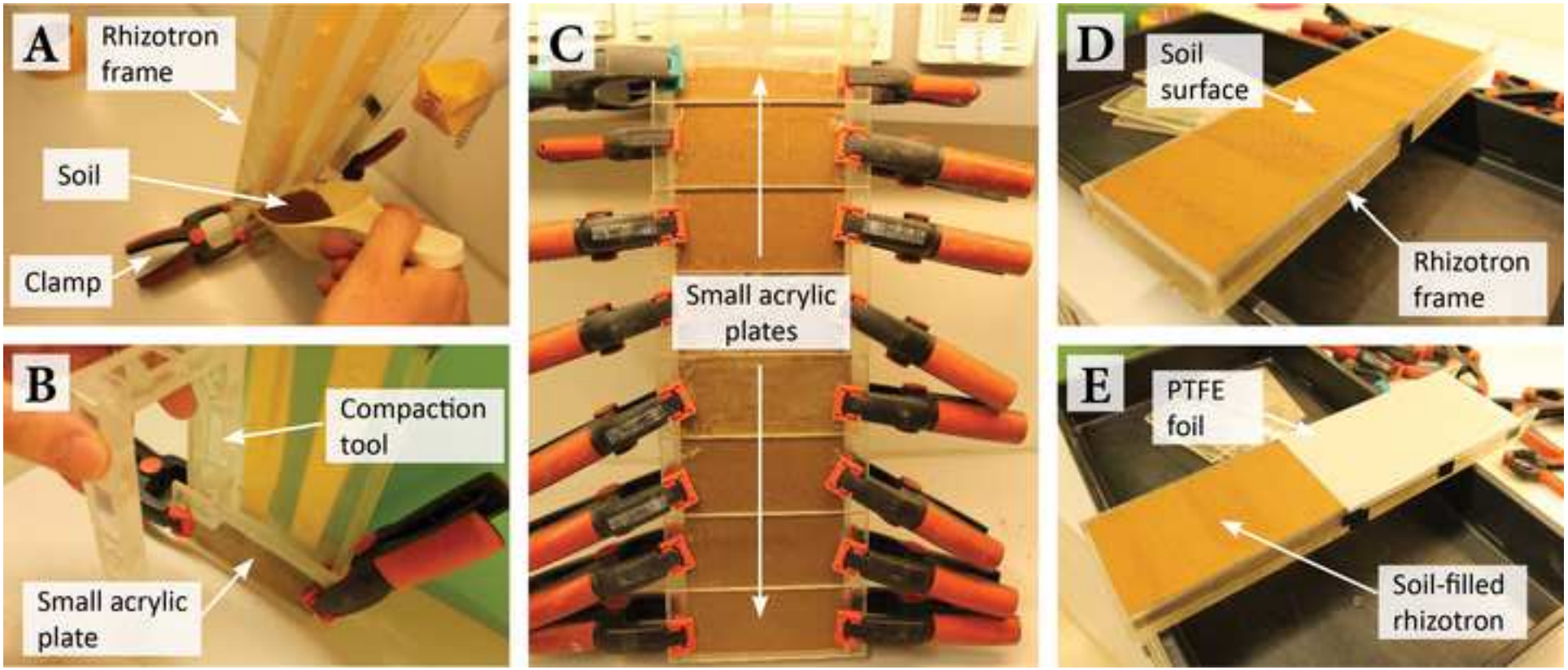

Figure 3

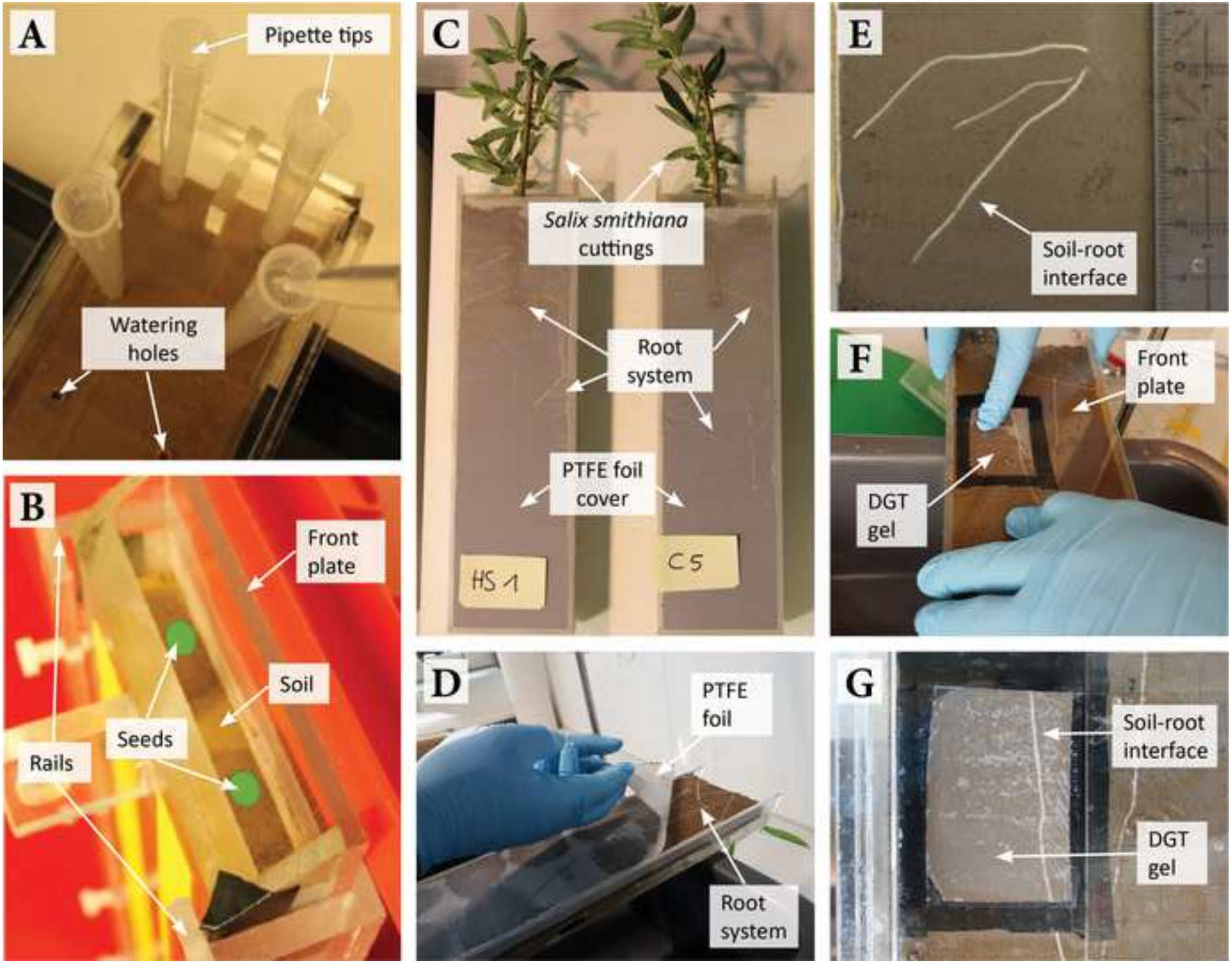

Figure 4

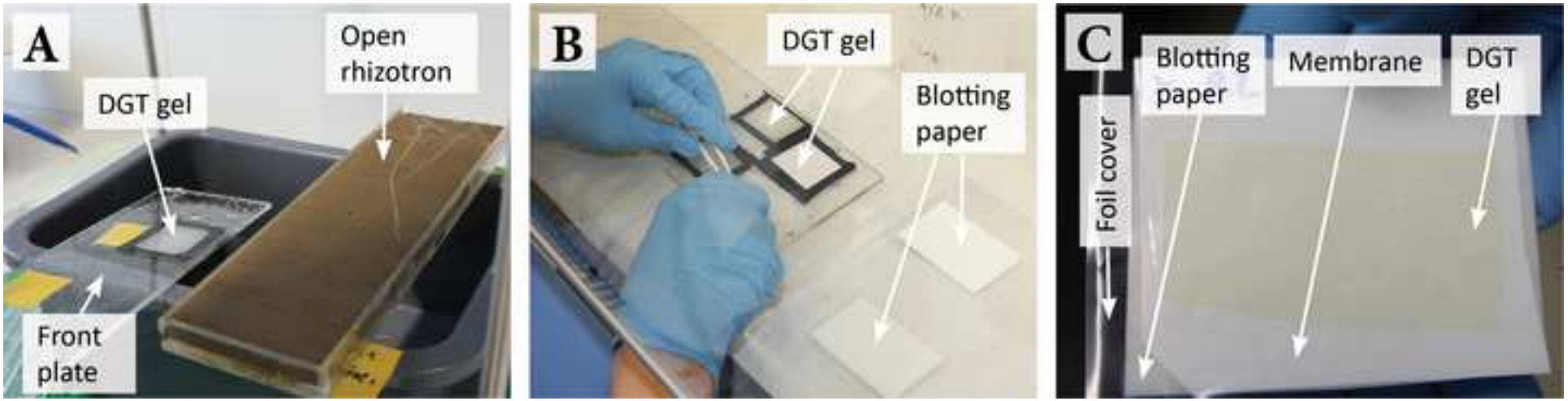

Figure 5

Click here to access/download;Figure;Figure5_LA-ICP-MS.jpg

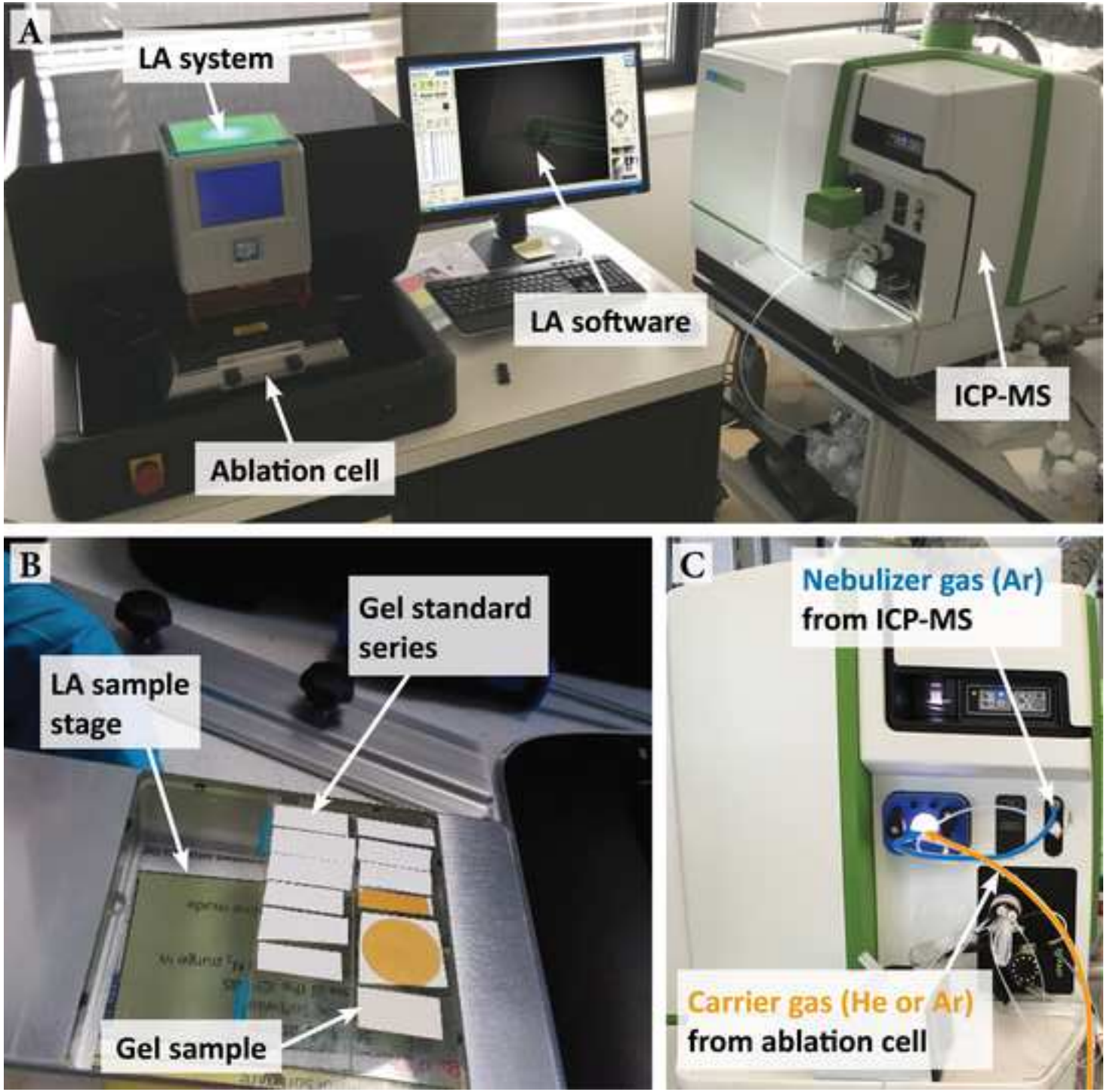

Figure 6

Click here to access/download;Figure;Figure6_DGT LA-ICP-MS line-scan imaging.jpg

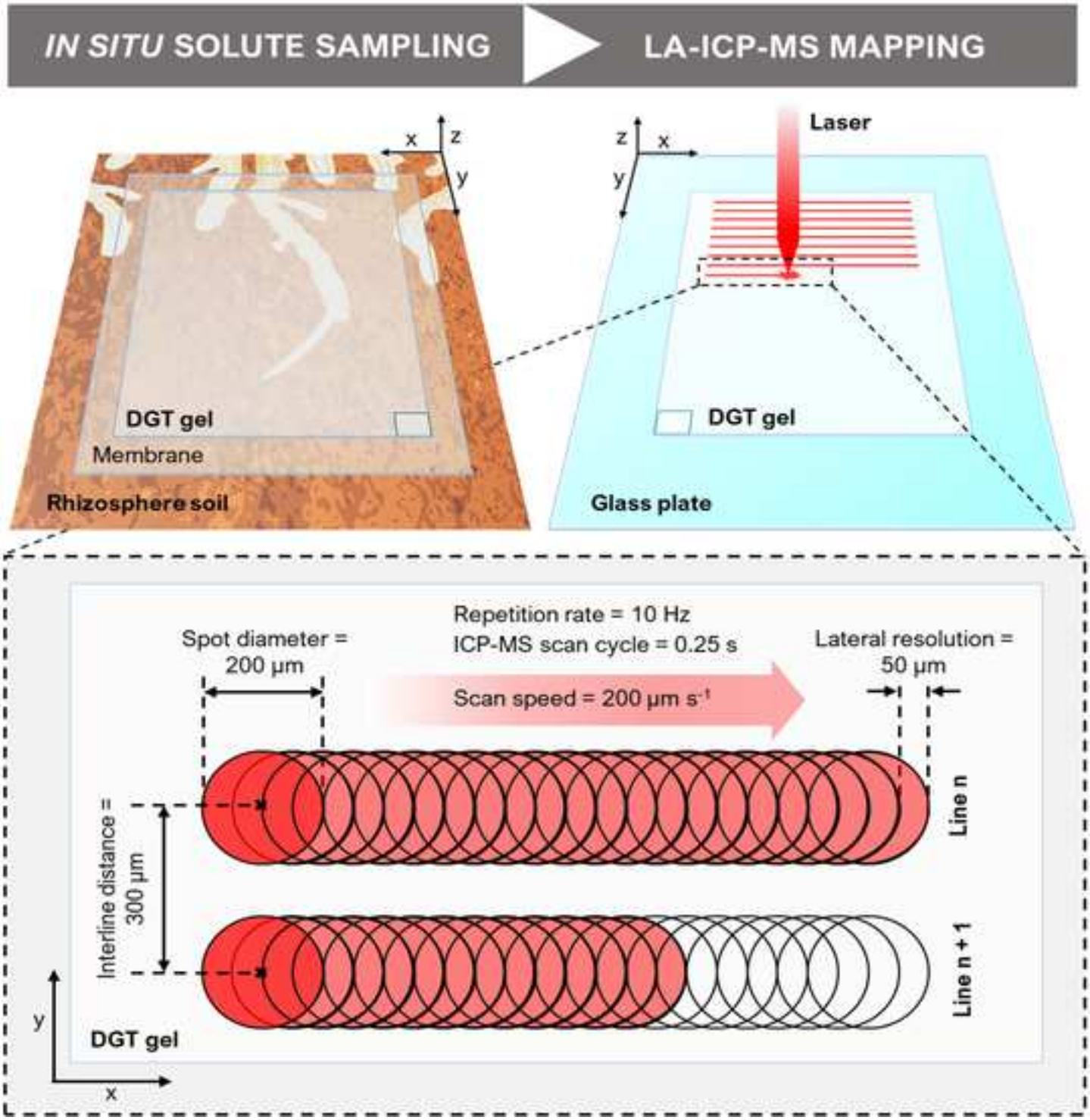

Figure 7

Click here to access/download;Figure;Figure7_representative results.jpg

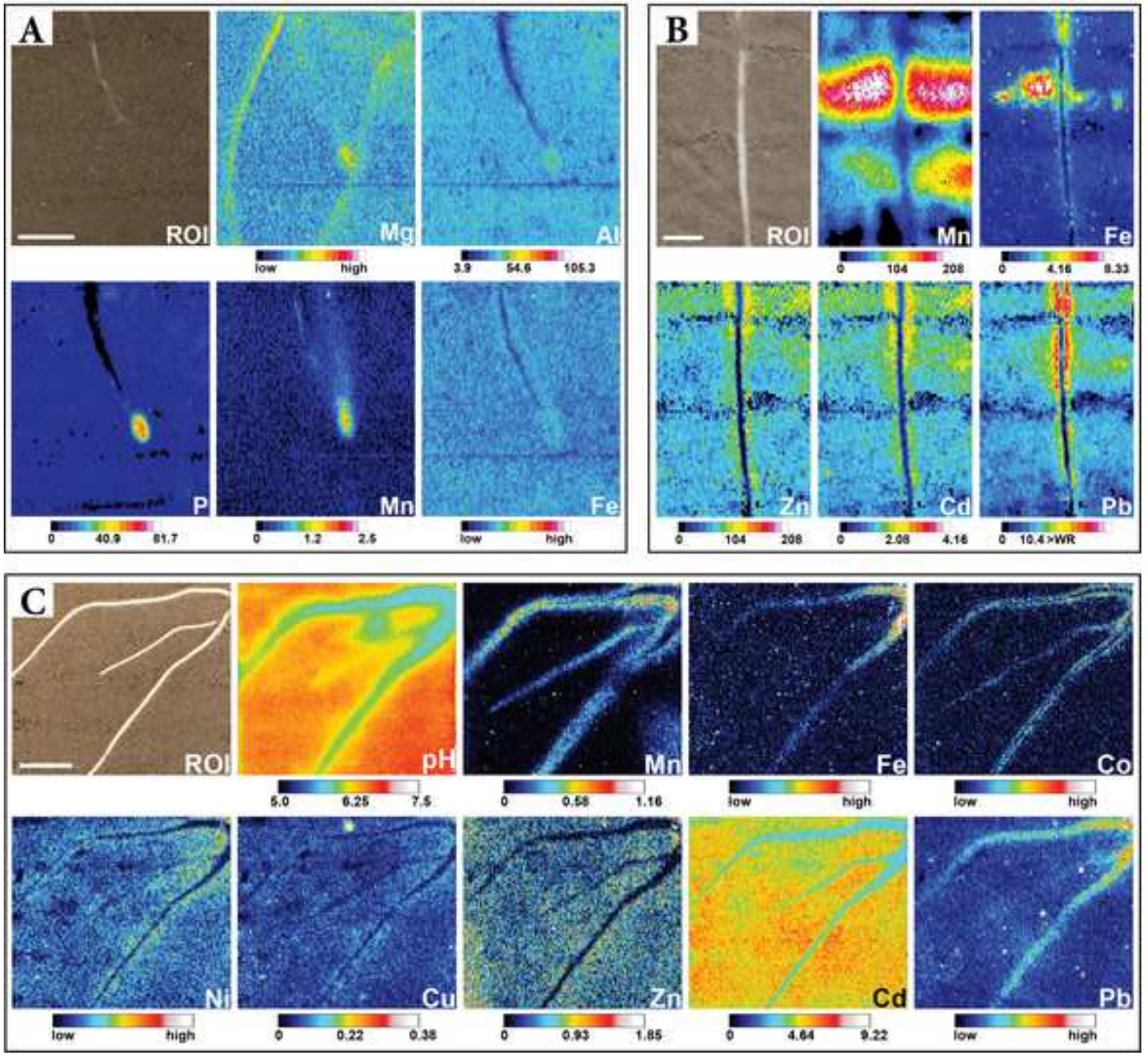

Table 1

DGT gel fabrication	**Plant cultivation**	**In situ solute sampling**	**LA-ICP-MS solute flux mapping**
HR-MBG *1 week*	Soil preparation *1 week*	Gel application *1 hour per gel*	Sample preparation *1 hour per gel*
HR-ABG *3 days*	Rhizotron assembly *2 hours per replicate*	Solute sampling period *variable, typically 24 hours*	LA-ICP-MS analysis *1 day per gel*
HR-CBG *3 days*	Plant growth *dependent on study*	Gel retrieval *1 hour per gel*	Data processing *4 hours per gel*
		Gel drying *2-3 days*	Image generation *30 min per image*

Name of Material/ Equipment	Company	Catalog Number
$(NH_4)_2S_2O_8$ (ammonium persulfate; APS)	VWR	21300.260
2-(N-morpholino)-ethanesulfonic acid (MES)	Sigma-Aldrich	M8250-100G
Acrylamide solution	Sigma-Aldrich	A4058-100ML
Analyte salts	n/a	n/a
Buechner funnel	VWR	511-0065
Chemical equilibrium modelling software	KTH Sweden	n/a
Clamp	Local warehouse	n/a
Desktop publishing software	Adobe Inc.	n/a
DGT cross-linker	DGT Research Ltd	n/a
DGT piston sampler	DGT Research Ltd	n/a
Digital single-lens reflex (DSLR) camera	Canon Inc.	n/a
Dispersion device	IKA	3737000
Double-sided adhesive tape	Tesa	56171
Ethanol	Sigma-Aldrich	34923
Gel blotting paper	Whatman	10426981
Gel drier	UniEquip	n/a
High-pressure microwave system	Anton Paar	n/a
HNO_3	VWR	1.00456.2500P
Horizontal shaker	GFL	305
HydroMed D4	AdvanSource Biomaterials Corp.	n/a
ICP-MS software	Perkin Elmer	n/a
Image analysis software	National Institutes of Health (NIH)	n/a
Knife-coating device	BYK	5561
LA software	Elemental Scientific Lasers	n/a
LA system	Elemental Scientific Lasers	n/a
Laminar flow bench	Telstar Laboratory Equipment B.V.	n/a
Magnetic stirrer	IKA	0003582400
Moisture-retaining film	Bemis Company, Inc.	PM999
N,N,N',N'-tetramethylethylenediamine (TEMED)	Sigma-Aldrich	T9281-50ML
$NaNO_3$	Sigma-Aldrich	229938-10G
NaOH	Sigma-Aldrich	1064980500

Overhead shaker	GFL	3040
Perfluoroalkoxy alkane (PFA) vials	Savillex	200-015-20
pH meter	Thermo Scientific	13-644-928
pH probe	Thermo Scientific	8157BNUMD
Plastic cutter	DGT Research Ltd	n/a
Plastic tweezers	Semadeni	602
Plasticine	Local stationary shop	n/a
Polycarbonate membrane discs	Whatman	110606
Polycarbonate membrane sheet	Whatman	113506
Polyethersulfone membrane discs	Pall Corporation	60172
Polyethersulfone membrane sheet	Pall Corporation	60179
PTFE foil	Haberkorn	n/a
PTFE spacer	Haberkorn	n/a
PTFE-coated razor blades	Personna GEM	62-0178
PTFE-coated Tygon tubing	S-prep GmbH	SP8180
Quadrupole ICP-MS	Perkin Elmer	N8150044
Quantitative filter paper, 454	VWR	516-0854
Spreadsheet software	Microsoft Corporation	n/a
Stainless-steel cutter	Local locksmithery	n/a
Suspended particulate reagent-iminodiacetate (SPR-IDA)	Teledyne CETAC Technologies	n/a
Transistor-transistor logic (TTL) cable	n/a	n/a
Two-volume cell	Elemental Scientific Lasers	n/a
Vinyl electrical tape	3M	n/a
Water purification system	Termo Electron LED GmbH	n/a
$ZrOCl_2 \times 8H_2O$	Alfa Aesar	86108.30

Comments/Description
≥98.0%, analytical reagent
≥99.5%
40%, for electrophoresis
Use water soluble analyte salts of analytical grade or higher
13 cm plate diameter
Visual MINTEQ
InDesign CS6
2%, agarose derivative
2 cm diameter exposure window
Canon EOS 1000D
Ultra-Turrax T10 Basic
Puriss. p.a., absolute, ≥99.8%
Blotting Papers, Grade GB005, 20 × 20 cm, 1.5 mm thickness
UNIGELDRYER 3545
Multiwave 3000
65%, ISO for analysis
Ether-based hydrophilic urethane
Syngistix
ImageJ Fiji, freely available at https://fiji.sc/
Single Bar 6”, 0.5 mils
ActiveView
NWR193
Class II biological safety cabinet
C-MAG MS 7
Parafilm M, 4" x 250'
BioReagent, suitable for electrophoresis, ~99%
99.995% trace metals basis
Pellets for analysis

15 mL Standard Vial, Rounded Interior
Orion 3-Star Benchtop pH Meter
Orion ROSS Ultra pH/ATC Triode
Use empty cross-linker vials from DGT research Ltd

non-drying plastic modelling mass based on paraffin wax and bulking agents
Nuclepore Hydrophilic Membrane, 25 mm diameter, 0.2 µm pore size, 10 µm thickness
Nuclepore Hydrophilic Membrane, 8 × 10 in, 0.2 µm pore size, 10 µm thickness
Supor 450 Membrane Disc Filters, 25 mm diameter, 0.45 µm pore size, 0.14 mm thickness
Supor 450 Membrane Disc Filters, 293 mm diameter, 0.45 µm pore size, 0.14 mm thickness
50 µm thickness
Variable thicknesses available
Stainless steel single edge blades (coated)
0.32 cm inner diameter
NexION 2000B
Particle retention 12-15 µm
Microsoft Excel 2016 (v16.0)
2.5 cm diameter
10 µm diameter polystyrene beads, 10 % (w/v) bead suspension
Consult ICP-MS technician to identify a suitable TTL cable for a specific instrument
Two-volume cell 1
Scotch Super 33+
TKA-GenPure
99.9 %, metals basis

Tulln, July 10th 2020

REF: JoVE61661, Response to reviewers

Dear Vineeta Bajaj,

We were very happy to receive such positive and constructive feedback on our manuscript entitled "**Two-dimensional visualization and quantification of labile, inorganic plant nutrients and contaminants in soil**". Please find a point by point response to all editorial and reviewer comments below.

We look forward to your positive response.

On behalf of all co-authors from Austria,

Yours sincerely,

Stefan Wagner and Jakob Santner

Editorial comments

Changes to be made by the Author(s):

1. Please take this opportunity to thoroughly proofread the manuscript to ensure that there are no spelling or grammar issues. The JoVE editor will not copy-edit your manuscript and any errors in the submitted revision may be present in the published version.

Done.

2. Please format the manuscript as: paragraph Indentation: 0 for both left and right and special: none, Line spacings: single. Please include a single line space between each step, substep and note in the protocol section. Please use Calibri 12 points

Done.

3. Please include a university/institution affiliation for the second author - Christoph Hoefer.

A university affiliation is now provided for Christoph Hoefer.

4. Please define all abbreviations during the first-time use.

Done.

5. Please ensure that the long Abstract is within 150-300-word limit and clearly states the goal of the protocol.

Done. Abstract is 271 words.

6. For in-text formatting, corresponding reference numbers should appear as numbered superscripts after the appropriate statement(s) without brackets.

Done.

7. Please ensure that all text in the protocol section is written in the imperative tense as if telling someone how to do the technique (e.g., “Do this,” “Ensure that,” etc.). The actions should be described in the imperative tense in complete sentences wherever possible. Avoid usage of phrases such as “could be,” “should be,” and “would be” throughout the Protocol. Any text that cannot be written in the imperative tense may be added as a “Note.”

Done.

8. The Protocol should contain only action items that direct the reader to do something.

Done.

9. Please ensure that individual steps of the protocol should only contain 2-3 actions sentences per step.

Done.

10. Please add more details to your protocol steps. Please ensure you answer the "how" question, i.e., how is the step performed?

Done in agreement with the reviewers' comments (see below).

11. There is a 10-page limit for the Protocol, but there is a 2.75-page limit for filmable content. Please highlight 2.75 pages or less of the Protocol (including headings and spacing) that identifies the essential steps of the protocol for the video, i.e., the steps that should be visualized to tell the most cohesive story of the Protocol.

Done.

12. There is a 10-page limit for the Protocol, but there is a 2.75-page limit for filmable content. Please highlight 2.75 pages or less of the Protocol (including headings and spacing) that identifies the essential steps of the protocol for the video, i.e., the steps that should be visualized to tell the most cohesive story of the Protocol.

See above.

13. Please obtain explicit copyright permission to reuse any figures from a previous publication. Explicit permission can be expressed in the form of a letter from the editor or a link to the editorial policy that allows re-prints. Please upload this information as a .doc or .docx file to your Editorial Manager account. The Figure must be cited appropriately in the Figure Legend, i.e. "This figure has been modified from [citation]."

Appropriate citation has been checked. The representative results (Figure 6) have been reproduced from previous publications, all of which are licensed under CC BY and therefore free to share and adapt under the given terms of conditions (https://creativecommons.org/licenses/by/4.0/).

14. Please include all the Figure Legends together at the end of the Representative Results in the manuscript text.

Done.

15. As we are a methods journal, please ensure that the Discussion explicitly cover the following in detail in 3-6 paragraphs with citations:

a) Critical steps within the protocol

b) Any modifications and troubleshooting of the technique

c) Any limitations of the technique

d) The significance with respect to existing methods

e) Any future applications of the technique

Done.

16. Please remove commercial terms from the text and from the figure and use generic term instead e.g., LA system, LA software etc.

Done.

Reviewers' comments

Reviewer #1

Manuscript Summary:

This manuscript reports a visual determination and quantification of inorganic contaminants and nutrients using LA-ICP-MS. The authors have achieved sub millimeter level spatial resolution and has effectively applied for to track nutrient and cations contaminant diffusion near the rhizosphere of terrestrial plants. The sampling was done using diffusive gradients in thin films (DGT) using rhizotrons prior to LA-ICP-MS analysis. It appears that many of the related research works have been previously presented in various publications and cited in this manuscript (i.e. see Ref 3 & 25). The novelty of this article is a detailed discussion and potential video presentation of methodological steps related to 2D visualization and quantification of contaminants or nutrients, and their migration through soil-root rhizosphere interface.

The paper is well written and rich content. The experimental design is well thought out. The results are visually very interesting. I believe this contribution is beneficial to the plant and soil science community. However, authors must attend to following queries and revisions so that the quality of the manuscript could be strengthened. This implies that the manuscript needs a major revision.

Thank you for the positive and constructive feedback on our manuscript.

Major & Minor Concerns:

Title: OK

Abstract: This is a fine summary of the article.

Thank you.

Line 43: Give few examples of these nutrient and contaminants.

Few examples for nutrients (e.g. P, Fe, Mn) and contaminants (e.g. As, Cd, Pb) were **added**.

Line 93: include the charge of the anion: NO3-

Thank you, charge was **added**.

1. Introduction:

Introduction is well written, analytical problems are defined and relevant bases are covered.

Thank you for the positive feedback.

2. Protocol:

Line 216: Fix_ S1 & S2

The sentences referring to the Supporting Information were **combined**. The new sentence reads now as follows: "*Laboratory procedures for trace element analysis, as well as detailed fabrication procedures of all presented HR-DGT gels are described in the Supporting Information (SI) section S1 and S2.*" (lines 213-215)

Line 221: Incorrect formula! Zirconium hydroxide formula is zirconium (IV) hydroxide, Zr(OH)4

Thank you, was **corrected** to "*zirconium (IV) hydroxide*" throughout the manuscript.

Line 224: spell out first HR-MBG

Abbreviations for the high resolution (HR)-DGT binding gels (HR-MBG, HR-ABG, and HR-CBG) **are now spelled out** before their first use.

Line 226: Zr(OH)4 or simply write zirconium (IV) hydroxide here as well as elsewhere.

Corrected, see comment above.

Line 228: What are these solids? Soil alone? anything else?

Yes, we refer to the mass of dry soil in the rhizotron. To clarify this, **we adapted the symbol and its definition**: "*the mass of dry soil in the rhizotron, $m_{d,soil\ rt}$ (g)*" (line 272). In response to the comment of Reviewer #3, we further added equation Eq. 1, showing the exact calculation of $m_{d,soil\ rt}$ (line 275).

Line 465: Can you do this experiment with 213 nm laser? Must address here. What are the limitations if any?

Yes, the analysis of DGT binding gels can be accomplished using lasers with a wavelength of 213 nm or also 266 nm. **This is now explicitly stated** in the protocol, lines 471-472: "*Alternatively, nanosecond 213 nm or 266 nm solid-state LA systems can be applied36,39-43.*" Generally, the laser wavelength is a primary control for the sample penetration depth (Gonzalez et al., 2002), as well as the particle size distribution of the generated aerosol (Guillong et al., 2003). Previous work where laser ablation of NIST glass standards using wavelengths of 193 nm, 213 nm and 266 nm was directly compared, while other LA-ICP-MS parameters were kept constant, demonstrated that 193 nm lasers generate the smallest particle size, leading to decreased noise and thus enhanced precision and stability of the transient signals (Guillong et al., 2003). Considering that the signal stability is a primary contributor to the combined measurement uncertainty (u_c) in LA-ICP-MS (Luo et al., 2007; Kreuzeder et al., 2015), the use of 193 nm lasers may improve the analytical precision in DGT ablation analysis. However, the typically ~2-fold higher uncertainty in LA-ICP-MS analysis of DGT gels (relative combined uncertainty (U_{rel}, k = 2) of 34.4-90.5%;) (Kreuzeder et al., 2015) compared to the uncertainty in LA-ICP-MS analysis of NIST glass standards (U_{rel} of 6.4-42.9%, k = 2) (Luo et al., 2007) indicates that the comparatively low signal stability in DGT LA-ICP-MS analysis is dominantly affected by other means such as the complex

polymer matrix and inhomogeneities in the embedded resin distribution (Kreuzeder et al., 2015). We therefore suppose that the effect of the laser wavelength on the measurement uncertainty is negligible in LA-ICP-MS analysis of DGT gels.

Line 497: Have you used He gas to enhance the signal? If so what is the volume? What are the limitations and advantages?

Yes, He was used as an aerosol carrier gas from the LA cell to the ICP-MS at a flow rate of 900 mL min^{-1}. The He gas stream was then mixed with an Ar gas stream from the ICP-MS via a two-way Y connector prior to its introduction into the ICP-MS. **This was also explicitly stated** in the Supporting Information chapter S5 ("*Coupling the LA system to the ICP-MS*"), lines 506-507 and lines 514-517: "*S5.2. Connect N2 as purge gas to 'N2 PRG GAS IN' and He as carrier gas to 'MFC 1 GAS IN' at the gas panel of the LA system.*"; "*S5.3. Connect the 'ONLINE GAS OUT' He carrier gas flow of the LA system and the 'NEB' Ar nebulizer gas flow of the ICP-MS to the ICP interface via a PTFE-coated Tygon tubing (Table of Materials) equipped with a two-way Y connector and a torch adapter fitting to the ICP injector (Figure 5C).*" In the associated note (lines 510-512), **we provide a reference** (Günther and A. Heinrich, 1999) for an in-depth discussion of the limitations and advantages of using He or Ar (or mixtures of both) as carrier gas in LA-ICP-MS: "*NOTE: The present protocol uses He as the aerosol carrier gas. Alternatively, Ar can be used as carrier gas. See Günther and Heinrich11 for a detailed discussion of the effects of using either He or Ar as carrier gas.*" We provide this information in the Supporting Information to keep the focus of the main manuscript protocol on the practical implementation of the 2D DGT sampling and the operations of the LA-ICP-MS line-scan imaging, assuming an already established LA-ICP-MS coupling.

Line 504-506: Give a typical example calculation here to a novice reader.

A typical example calculation **was added**. This reads now as follows (lines 510-511): "*For example, when setting a spot diameter of 200 µm and a total ICP-MS scan cycle duration of 0.25 s, the scan speed should be ≤800 µm* s^{-1}*.*"

Line 512-513; Include a line pattern in a cartoon figure.

Thank you for pointing out that a schematic representation of the line-scan pattern was missing. **We prepared a new Figure (Figure 6)**, which will help the reader to better understand and visualize the associated dimensions and parameters:

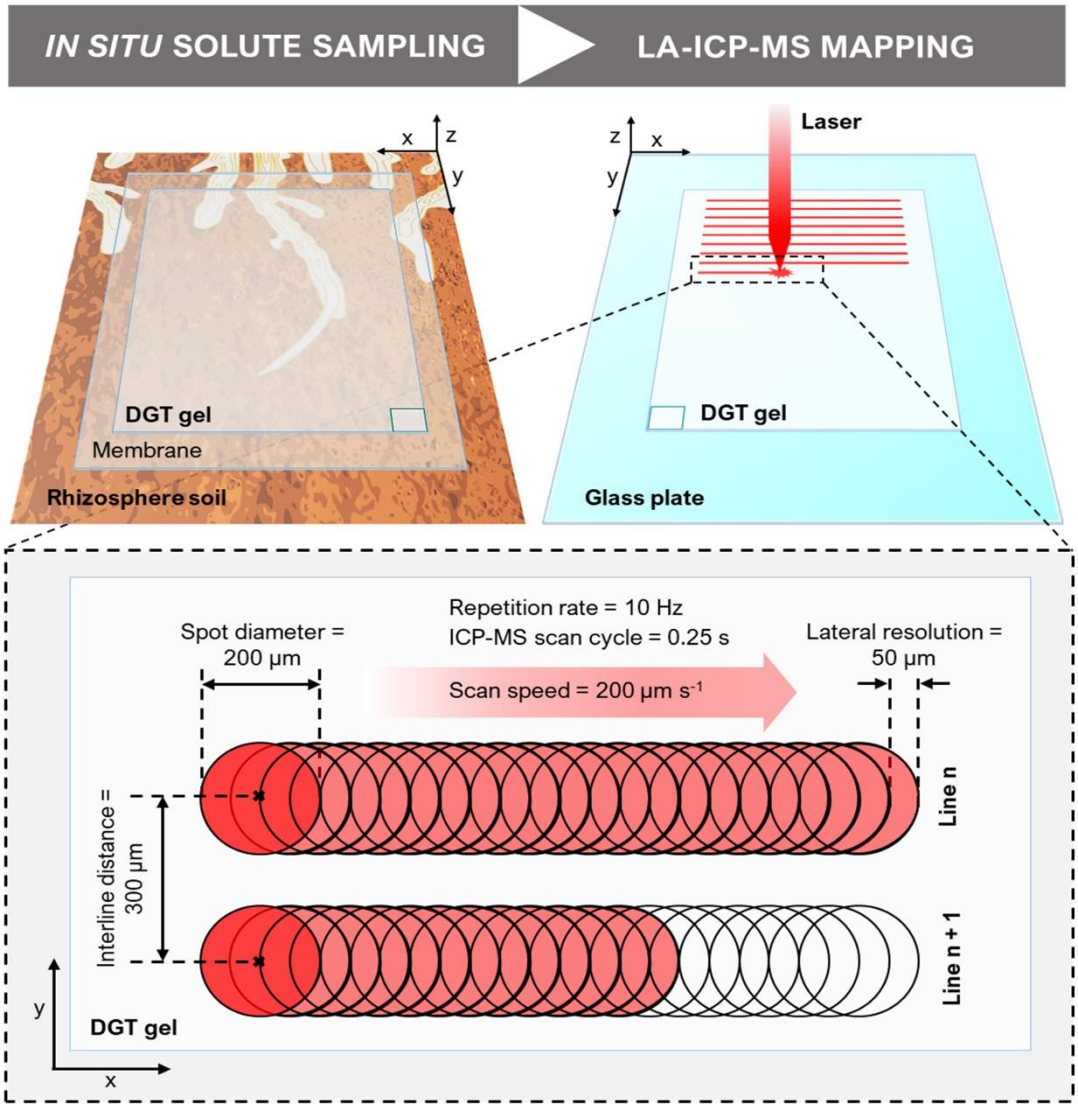

"***Figure 6: Schematic of the DGT LA-ICP-MS experimental design (not to scale).*** *The illustration depicts the DGT-based in situ solute sampling in the rhizosphere and the LA-ICP-MS mapping of the solute distribution on the gel surface, including a close-up showing exemplary line-scan dimensions and parameters. Note that the DGT gel is horizontally flipped when transferred from the rhizosphere soil onto the glass plate, as indicated by the position of the rectangle at the bottom corner of the DGT gel.*"

Line 520-522: Suggestion: Give an example or show in the video clearly.

An example **is now provided** in the new line-scan figure (Figure 6).

Line 525: Some LA-ICP-MS literature say 13C is not a good internal standard. Any comments? also and address this issue?

Internal standardization of the analyte signals with a stable reference signal can be effective in improving the analytical precision by correcting for temporal changes in the measurement condition and resulting sensitivity drifts. This is particularly important in DGT ablation analysis because

measurement times of individual DGT gels are significant (typically 3-6 h for gel areas of 5-15 cm^2) and replicate measurements may be performed over the course of several days or weeks.

Carbon is a major component in biological materials and polymers and therefore one of the most applied elements for signal normalization in LA-ICP-MS (Walas et al., 2014). In DGT gels, carbon represents the major matrix element accounting for ~41 and ~51 mass percent in the polyurethane and polyacrylamide matrix, respectively. Several studies have demonstrated that ^{13}C is well applicable for internal normalization in the LA-ICP-MS analysis of the HR-MBG (Kreuzeder et al., 2013; Kreuzeder et al., 2018; Wagner et al., 2020), HR-ABG (Guan et al., 2015) and HR-CBG gels (Gao and Lehto, 2012; Lehto et al., 2012; Williams et al., 2014; Hoefer et al., 2015; Lehto et al., 2017). The approach gives relative standard deviations (RSD) for ^{13}C over 10 mm line-scan ablations of typically ~5% (S. Wagner, J. Santner and T. Prohaska, manuscript in preparation).

An alternative approach is to use dual-layer DGT gels where a second gel layer underneath the actual sample gel is loaded with known amounts of internal standard elements (Warnken et al., 2004a). Laser parameters are adjusted to ensure penetration of the laser beam through the first gel layer and thus ablation of both gel layers simultaneously. Using this approach, Warnken et al. (2004a) evaluated the use of Sc, In, Ba, La, Ce and Tb as internal standards. Of the investigated elements, Ba showed the best precision (≤10%) but could not be used as an internal standard due to its relatively high and variable presence in natural soils and sediments. Therefore, ^{115}In was applied for internal standardization, showing a substantially higher RSD (~10%) compared to ^{13}C, indicating that the preparation of spiked dual-layer DGT gels is unnecessarily complex. Moreover, the dual-layer DGT approach requires spot ablation to ensure penetration through the sample gel into the internal standard gel. Line-scan ablation is not possible, thereby leading to a decreased lateral resolution, decreased sensitivity, increased limits of detection and a 30% increase of the measurement time and gas consumption of the analysis (Gao and Lehto, 2012). Moreover, the introduction of additional sample preparation steps will generate additional sources of uncertainty in DGT ablation analysis.

In conclusion, internal normalization using ^{13}C is the method of choice in high resolution DGT LA-ICP-MS analysis to date. The different approaches for internal normalization in DGT LA-ICP-MS analysis have been discussed in detail in previous reviews on the DGT LA-ICP-MS technique (Santner et al., 2015; Santner and Williams, 2016). We therefore prefer not to re-address this issue in this method protocol.

Line 560-561: Why explain? How to minimize these laser fluency variations? Explain to the audience.

The laser fluence, or energy density, is the total energy contained within the laser light per unit area (J cm^{-2}) and thus determines the energy arriving at the sample surface. The stability of the laser fluence

thereby directly reflects the stability of the material ablation process, i.e. the higher the variation in laser fluency, the higher the variation in the amount of ablated material. If the laser fluency would be highly variable, this would either indicate a degraded laser source and/or mirror system, leading to variable energy densities arriving at the sample surface. Laser fluency variations can be effectively minimized by regular technical service of the laser source and mirror system. To provide this context for the reader, **we added the following sentence** to the protocol, lines 566-568: "*4.2.15. Monitor the laser fluence (J cm-2) during analysis to assess the laser stability. If the fluence varies largely, abort the analysis and verify that the laser source and/or its mirror system are fully functional.*"

Line 588: ... intensity ratio... This ratio is a unitless (a dimensionless quantity) parameter

Thank you, the unit was **removed**.

Line 589: …compute the calibration function (y =ax + b) using a linear regression…

Thank you, "($y = ax + b$)" was **added**.

Line 594: … notice cps cps-1 cancels out! Thus, a unitless parameter_ Fix.

Thank you, the unit was **removed**.

Line 615-618: Include a cartoon of this scan depicting these dimensions and conditions.

A line-scan cartoon figure (Figure 6) was added. The dimensions and conditions in the text were slightly adapted to match with those shown in Figure 6.

Representative Results/Discussion

Although, it appears that the material has been presented in various publications previously but this is a good discussion for a "how to do type video journal article." It also discusses advantages, limitations, artifacts and practical hints to improve rhizotron studies, including potential pitfalls.

Line 859: Correct this dimensionless parameter: Pb images show 13C-normalized intensity ratio (cps cps-1).

Thank you, the unit was **removed**.

Line 861; include copyright clearance numbers and citations clearly here: …. are reproduced from the cited articles (Refs) licensed under CC-BY

Thank you, **citations were added** to make this clearer.

Figs. 2 & 3 label important devices/parts in Figs 2&3 just like you did in Fig. 1

Important components in Figures 2, 3 and 4 **are now labelled**:

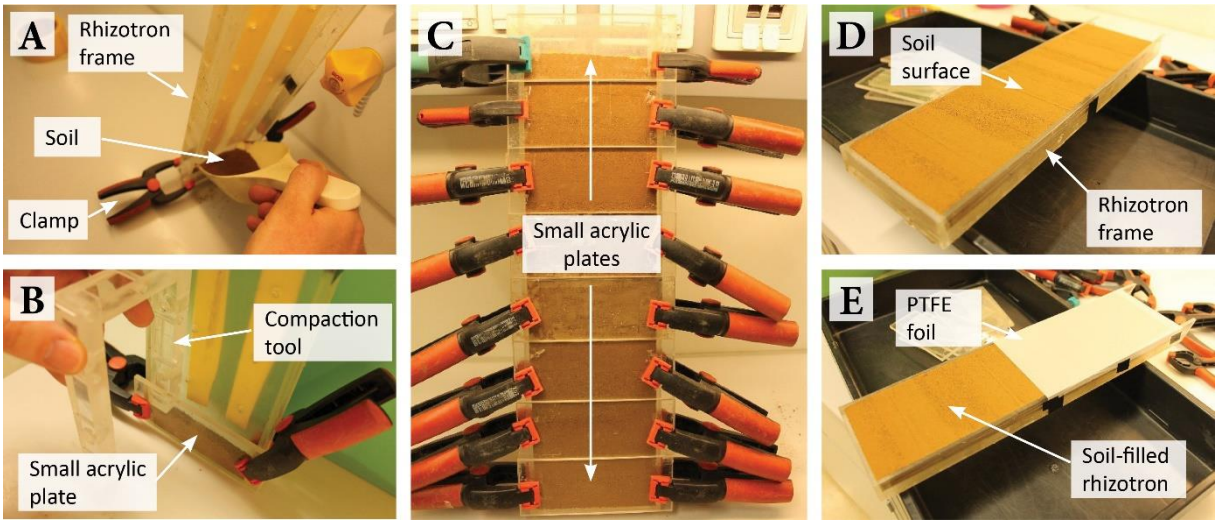

"***Figure 2: Rhizotron assembly and filling to grow plants in soil for solute imaging in the rhizosphere.*** *(A) Soil filling into the rhizotron. (B) Compaction of the filled soil using a compaction tool. (C) Soil-filled rhizotron with small acrylic plates and clamps. (D) Soil-filled rhizotron with exposed soil surface. (E) Soil-filled rhizotron with a protective PTFE and plastic foil cover.*"

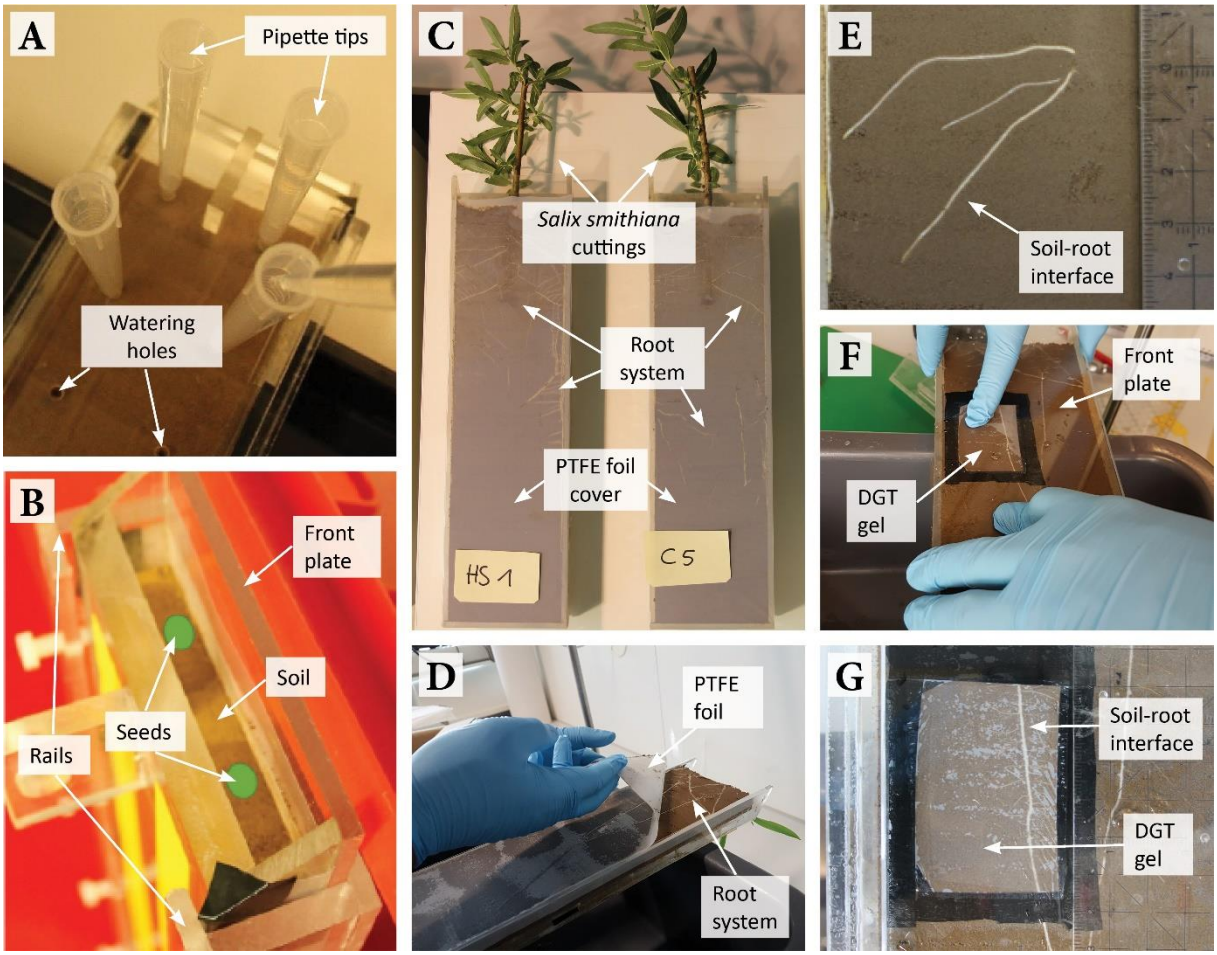

"*Figure 3: Rhizotron handling and DGT gel application.* (A) Soil watering using 10 mL pipette tips in the watering holes in the back of the rhizotron. (B) Planting of seedlings (indicated as green spots) into the soil-filled and closed rhizotron. (C) Rhizotron planted with Salix smithiana cuttings and removed front plate and plastic foil cover. (D) Carefully peeling off the PTFE foil cover before DGT gel application. (E) High-resolution photo of the soil-root interface ROI. (F) Application of the front plate equipped with the DGT gel onto the rhizotron. (G) Photo of the ROI with the DGT gel applied during solute sampling."

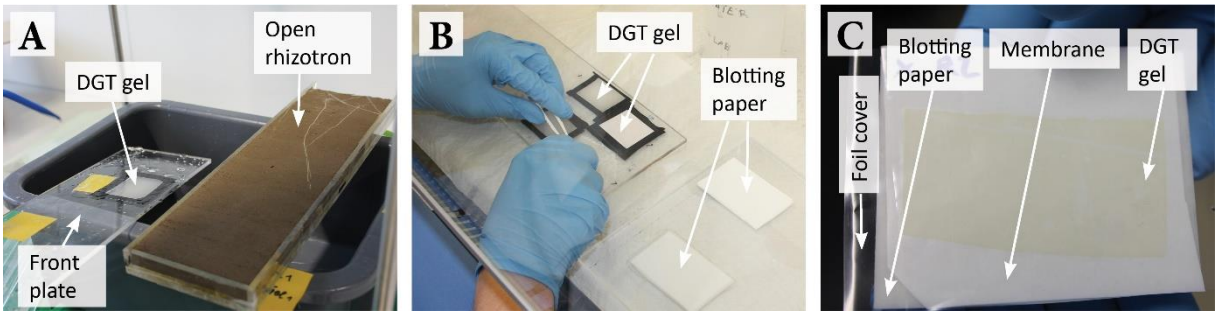

"*Figure 4: DGT gel retrieval and preparation for drying upon solute sampling.* (A) Plate with the DGT gel and rhizotron directly after solute sampling. (B) Retrieval of the DGT gel from the plate in a laminar flow bench. (C) Stack of gel blotting paper/polyethersulfone membrane/DGT gel/plastic foil cover for gel drying. Note that the gel is slightly colored after its deployment on soil."

Reviewer #2

Manuscript Summary:

In this manuscript, the authors described an effective method to visualize and quantify inorganic nutrient and metal elements in soil adjacent to plant roots by combing the technologies of DGT and a highly sensitive LA-ICP-MS. The details for making DGT gels, cultivating plant, sampling of solute and chemical analysis were well explained. This method can be widely used to visually quantify inorganic elements in various fields.

Thank you for the positive feedback.

Minor Concerns:

How can you ensure the samples you concerned were totally bound to the gel?

Quantitative sampling of labile anionic and cationic solutes by the presented DGT gels has been characterized and validated in detail in the original gel development publications (Warnken et al., 2004b; Kreuzeder et al., 2013; Guan et al., 2015). This published data shows linear accumulation of the target solute species over time if the resin binding sites in the DGT gels are not saturated. **This aspect is explicitly stated** in the Supporting Information, lines 335-336: "*Verify that the total gel analyte*

loading (i.e. $\sum \Gamma_{DGT}$*) of the highest calibration standard is well below the total analyte binding gel capacity (≤80 %).*" Thus, we ensure quantitative solute sampling by maintaining the total DGT gel analyte loading below 80 % of its total analyte binding capacity.

Reviewer #3

Manuscript Summary:

The authors describe in detail the method for 2D visualization of elements (e.g., inorganic nutrients and contaminants) in soil using diffusive gradients in thin films (DGT) and laser ablation inductively coupled plasma mass spectrometry (LA-ICP-MS). The spatial resolution is sub-mm, which enables inspection of the rhizosphere. Images can be quantitative by relative normalization within the sample or compared to an external standard, creation of which is described within the text. It appears that a reader could follow these steps and attain the results suggested. This detailed method and photographs will be greatly helpful for others that would like to use DGT. The method can complement other methods/applications described in the literature, and will be useful for investigating soil rhizosphere questions.

Thank you for the positive feedback.

Major Concerns:

In regard to controls, is there a way to check that DGT is working as anticipated (or in contrast, did not work correctly)? Are there checkpoints along the way that authors can suggest to assure the method (e.g., preparation of gels) was done correctly (e.g., to mimic soil/nutrient diffusion system)? For example, if at the end the images do not produce expected are there ways the reader could assess that they performed the method correctly (i.e., discern error made in the method vs. result of the specific soil system).

The correct chemical functionality of the DGT imaging technique can be verified by several means:

1) Correct gel preparation can be simply checked by visual inspection of the fabricated gels for areas of inhomogeneous material distribution. If prepared correctly, the binding gels enable quantitative sampling of the target solute species if the gel loading is kept below capacity thresholds (Davison, 2016).

2) Quantitative solute sampling is verified during the DGT standard preparation experiment as outlined in the Supporting Information, chapter S4 ("*Preparation of DGT LA-ICP-MS calibration standards*"). Here, gel standards are prepared in quadruplicates by controlled loading of the DGT gels with the

target analytes following the DGT theory based on Fick's first law of diffusion (Davison, 2016). The analyte loading is then assessed in three gel replicates by gel elution (HR-ABG and HR-CBG) or complete digestion (HR-MBG) followed by analyte quantification using an established analytical technique (e.g. ICP-MS) in combination with metrological validation using certified liquid reference materials. If the experimentally determined gel loading differs largely from the targeted gel loading, this indicates that the DGT gels are not working correctly. The remaining gel replicate is dried and then used as a matrix-matched reference gel with known analyte loading for LA-ICP-MS analysis.

3) Correct sample preparation (drying, mounting on glass plates) for LA-ICP-MS analysis can be verified by testing the analytical performance of standard gels. If prepared correctly, the detected LA-ICP-MS line-scan signal intensity of gel standards should be clearly distinguishable from the gas blank and method (gel) blank background signal, especially for high analyte loadings. If unable to obtain a signal that can be distinguished from the background, the reader must ensure that all protocol steps were performed correctly. Sometimes, the DGT gel is accidentally flipped after solute sampling with the loaded, soil-exposed side facing towards the glass plate rather than the laser beam, resulting in low signal intensities and erroneously flipped features in the final solute flux image.

4) Detectability of solutes bound to the gel from a specific soil can be tested using bulk DGT piston sampling in preliminary experiments (Hooda et al., 1999; Smolders et al., 2020).

This information is now provided in the Discussion, lines 852-874: "*Another important consideration is the chemical functionality of the fabricated DGT binding gel. By following the protocol, thin gels with a homogeneous distribution of binding phases are obtained. If the gels have areas of inhomogeneous material distribution (e.g. holes in the gel or aggregates of binding phases) these areas need to be removed or, if too extensive, the gel fabrication protocol needs to be repeated. If prepared correctly, the gel must be able to bind the solutes that diffuse into the gel immediately and quantitatively27, which is determined by the specific gel binding capacity. While exceeding the gel capacity is less problematic in uncontaminated soils, it should be considered in metal-contaminated soils and saline soil environments. Thus, if very high quantities of labile nutrient/contaminant species are expected in the target soil environment, preliminary tests should be performed. For estimating expected DGT loadings, bulk soil DGT piston sampling followed by gel elution and wet-chemical analysis can be applied15,49. If necessary, DGT deployment times may be adjusted to reduce the gel contact time and thus avoid gel saturation above capacity thresholds. Preliminary tests can also be helpful to verify gel functioning and to adjust contact times if very low solute loadings are expected. Quantitative sampling of the target solute species can be further verified by controlled loading of DGT gels in the preparation of DGT LA-ICP-MS calibration standards. The gel standard provides a matrix-matched reference gel*

analyte loading that can be used to assess if the sample gel loading determined by LA-ICP-MS is within the expected range. If unable to obtain a signal which is different from the gas and method blank background noise, the operator must ensure that all protocol steps were performed correctly. Sometimes, the DGT gel is accidentally flipped after solute sampling with the soil-exposed, loaded side facing towards the glass plate rather than the laser beam, resulting in low signal intensities and erroneously flipped features in the final solute flux images."

Also, I realize method time can vary, but it could be helpful to outline approximate times for general steps to provide context for the reader. E.g., this is a method you could implement in a day, a week, over the course of a month; this step may take several hours. A general timeline (e.g., a table or figure) could be helpful.

A new table was prepared showing approximate times for general steps of the method. The table (Table 1) was included in the Representative Results, lines 647-648: "*Approximate times for general steps of the protocol are presented in Table 1. [Place Table 1 here]*"

"*Table 1: Approximate times for general steps of the DGT LA-ICP-MS technique.*"

DGT gel fabrication	**Plant cultivation**	***In situ* solute sampling**	**LA-ICP-MS solute flux mapping**
HR-MBG *1 week*	Soil preparation *1 week*	Gel application *1 hour per gel*	Sample preparation *1 hour per gel*
HR-ABG *3 days*	Rhizotron assembly *2 hours per replicate*	Solute sampling period *variable, typically 24 hours*	LA-ICP-MS analysis *1 day per gel*
HR-CBG *3 days*	Plant growth *dependent on study*	Gel retrieval *1 hour per gel*	Data processing *4 hours per gel*
		Gel drying *2-3 days*	Image generation *30 min per image*

I made suggestions for additional methods and references to include in introduction/discussion to provide context for the reader.

Specific comments:

Line 140: DGT is not the "only technique capable of multi-element mapping of nutrients and contaminants". It would be worth mentioning the high-resolution elemental mapping method of laser-induced breakdown spectroscopy (LIBS) [Ilhardet et al. 2019, SBB], perhaps in the prior paragraph, and

rephrasing this line for clarification. [Similar comment for lines 732-735, DGT may be one of the few but is not the only method.]

Thank you for highlighting that this point was not elaborated in sufficient detail. The sentence in line 140 was misleading, as it was not our intention to state that DGT is "the only technique capable of multi-element mapping of nutrients and contaminants". Yet, the DGT technique is unique in its ability to selectively sample labile (i.e. reversibly adsorbed) solute species *in situ* and at high spatial resolution while preserving the original solute distribution in the intact soil-rhizosphere-root system (Oburger and Schmidt, 2016; Santner and Williams, 2016). To the best of our knowledge, this is not possible with other solute sampling methods available to date. The combination of the DGT-based passive sampling approach with chemical mapping by LA-ICP-MS further enables the targeted 2D visualization of these labile, plant-available element fractions. Thereby, the DGT LA-ICP-MS technique differs from the method presented by Ilhardt et al. (2019), where LIBS was used to analyze total element distributions in soil-root samples extracted from rhizotrons by sampling soil cores followed by careful sample preparation to preserve the natural element distribution. This method is well suited to be combined with the DGT LA-ICP-MS technique, complementing the DGT solute flux and elemental speciation data with detailed information on mineralogy and solid phase trace element patterns in the soil-rhizosphere-root system.

To clarify the targeted solute sampling approach by DGT and its distinction from other techniques, **we corrected** the corresponding paragraph in the main manuscript, lines 147-150: "*The only technique capable of targeted 2D sampling of multiple nutrient and contaminant solutes at high spatial resolution is the diffusive gradients in thin films (DGT) technique, a sink-based sampling method that immobilizes labile trace metal(loid) species in situ on a binding material embedded in a hydrogel layer26,27."*

The method of Ilhardt et al. (2019) was added (Ref 25) to the introduction, lines 142-145, as another example for chemical imaging techniques applied in rhizosphere research: "*More recently, P. D. Ilhardt, et al. 25 presented a novel approach using laser induced breakdown spectroscopy (LIBS) to map 2D total multi-element distributions in soil-root core samples where the natural element distribution was preserved by careful sample preparation."*

Line 243: It could be helpful to provide references by other authors (some may have already been cited elsewhere in the manuscript) that show rhizotron setups, as designs can vary. The diagrams in this manuscript for how to craft rhizotrons will make it a lot easier for future readers to emulate the method.

The review of Luster et al. (2009) was **added**. In this reference several examples for different rhizotron studies are provided.

Line 273: "calculate the weight of dry soil in the rhizotron". How is this calculated?

The calculation of the mass of dry soil in the rhizotron, $m_{d,soil\ rt}$, **is now explicitly stated in equation Eq. 1**, which was added and reads as follows: "*(Eq. 1)* $m_{d,soil\ rt} = m_{m,soil\ rt} - m_{m,soil\ rt} \times w_{soil}$" (line 275). Here, $m_{m,soil\ rt}$ is the mass of moist soil in the rhizotron, and w_{soil} is the gravimetric water content of the pre-moistened soil.

Line 359: Any suggestions on how to account for the weight of the plant biomass?

Compared to the weight of soil in the rhizotron, long-term experience from our group has shown that the weight of the plant biomass is typically not significant in rhizotron studies. However, if significant, the weight of plant biomass could be accounted for by growing plants in separate rhizotron replicates and periodic harvest of the tissues at defined intervals. **This information is now provided** in the protocol, lines 360-363: "*Note: If plants are grown for extended periods and the plant biomass is expected to substantially decrease the amount of water added to the rhizotron by the proposed method, account for the weight of the plant biomass by growing plants in separate rhizotron replicates and harvesting and weighing the plant tissues at defined intervals.*"

Line 732-735: See comment on Line 140. DGT may be one of the few but is not the only method.

See our response above. **The paragraph was corrected** for clarification (lines 821-825): "*The solute imaging protocol presented here is a versatile method to visualize and quantify nutrient and contaminant fluxes in soil environments. It is unique in its capability to generate multi-element, 2D images of labile solute species in the soil/rhizosphere environment at sub-mm resolution, exceeding the achievable spatial resolution of alternative methods for measuring solute gradients in the rhizosphere substantially4.*"

Line 785: Another complementary diffusion-based imaging example to include is the fluorescent indicator imaging technique that was recently published: Lin et al. 2020, SBB, Non-destructive spatial analysis of phosphatase activity and total protein distribution in the rhizosphere using a root blotting method. It looks like this method would be a helpful addition to the introduction (perhaps as another method in lines 129-138).

Thank you for this reference. **The method by Lin et al. (2020) was added (Ref 24)** to both the introduction and the discussion:

Introduction, lines 135-137: "*Planar optodes are capable of imaging important soil chemical parameters such as pH and pO217-19, and enzyme activity or total protein distributions can be mapped using soil zymography20-23 and fluorescent indicator imaging based on root blotting methods24.*"

Discussion, lines 890-893: "*In addition to DGT-only applications, the method can be combined with other, diffusion-based imaging techniques like planar optodes3,33,42,43,48,51 and zymography20-24 (C. Roschitz, W.W. Wenzel, J. Santner et al., under review), and may be developed further for including additional elements and soil parameters.*"

Line 786: Rather than self-citing unpublished data on zymography, citing published literature by other authors would be appropriate. Work by Spohn et al. 2013 (ref 19), and there is additional literature since then using zymography, for example, Heitkotter and Marschner 2018, SBB.

Our intention was to cite a study, where DGT LA-ICP-MS solute imaging has been actually combined with zymography to enable simultaneous multi-parameter visualization. The cited manuscript was reviewed by *Soil Biology and Biochemistry* and we are currently working on revising the paper for publication in SBB. We will resubmit this manuscript shortly. Therefore, we would like to keep this citation. However, works by Spohn et al. (2013), Spohn and Kuzyakov (2014), Heitkötter and Marschner (2018), Guber et al. (2019), and Lin et al. (2020) (Refs 20-24) **are now included in the Discussion**, lines 890-893: "*In addition to DGT-only applications, the method can be combined with other, diffusion-based imaging techniques like planar optodes3,33,42,43,48,51 and zymography20-24 (C. Roschitz, W.W. Wenzel, J. Santner et al., under review), and may be developed further for including additional elements and soil parameters.*"

Minor Concerns:
Line 291: Define PTFE when first mentioned.

Corrected to: "*polytetrafluoroethylene (PTFE)*" (line 291)

Line 373: At the first mention of "laminar flow bench", it would be helpful to include the purpose of this specifically. For example, Supplemental line 56: "or any other dust- and metal-free environment."

Corrected to: "*Transfer the plate into a laminar flow bench (Table of Materials) or any other dust- and metal-free environment, unmarked side facing up.*" (lines 377-378)

Line 569: Define "cps" unit.

The unit "cps" was defined at its first appearance in the protocol, i.e. before line 569. The corresponding text (lines 562-563) reads as follows: "*4.2.14. Click 'Run' in the 'Run experiment' window*

to start the line-scan analysis and monitor the raw signal intensity in counts per second (cps) for each isotope on the ICP-MS in real time."

Figure 6: Be aware that for figure resolution, the text associated with the color scales was difficult to read. However, opening up the .jpg file directly was fine (this more high-resolution image would be better for the final version).

Thank you for the information, **the text font was slightly enlarged** for better readability:

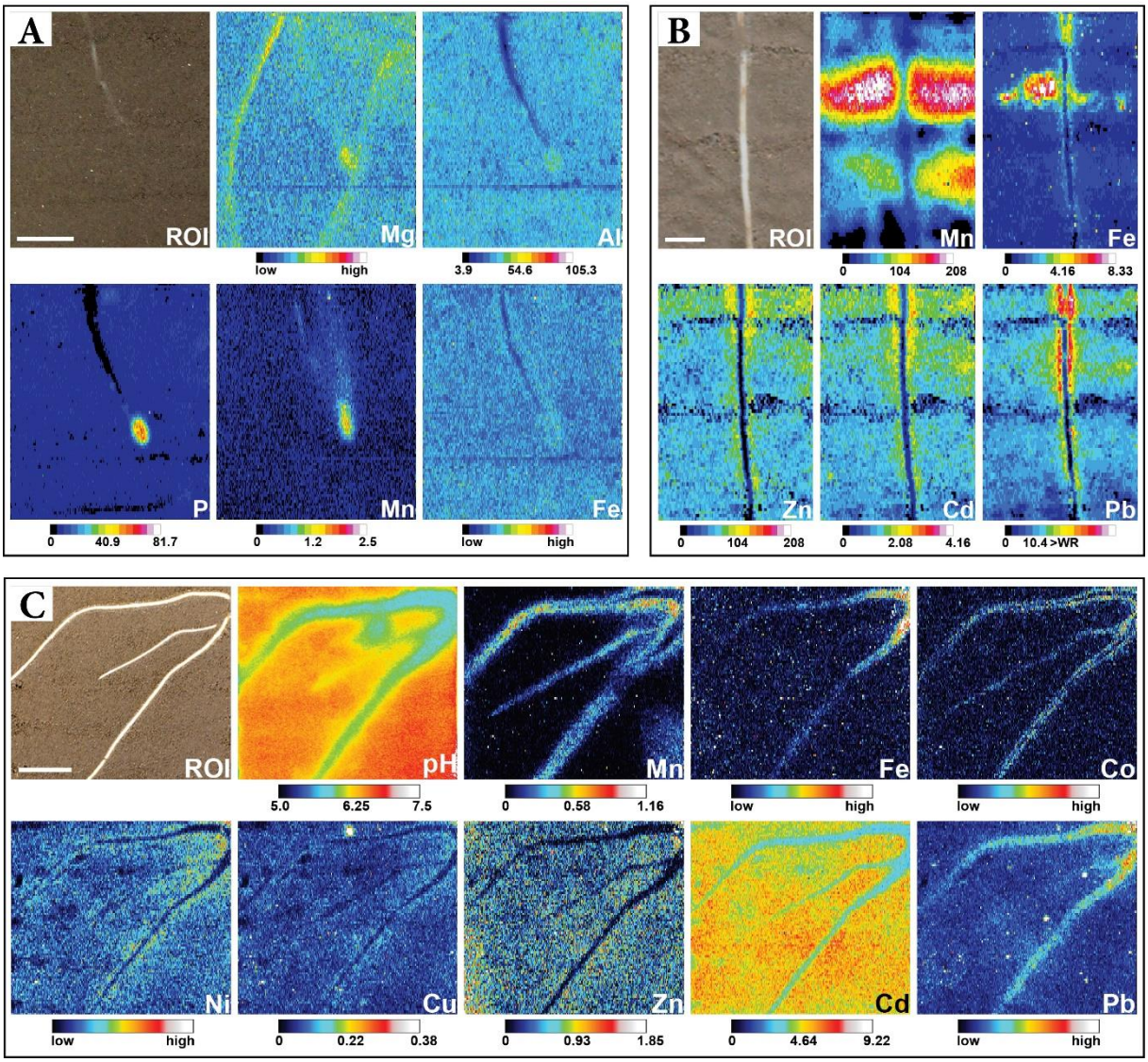

"***Figure 7: Sub-mm 2D distribution of labile nutrient and contaminant species across soil-root interfaces.*** *(A) Distribution of anionic P and cationic Mg, Al, Mn and Fe solutes around a young F. esculentum root. Co-localized sampling of anionic and cationic solutes was achieved using HR-MBG for 24 h at a soil water saturation of ~75 % WHC. The Al, P and Mn images are displayed as calibrated fDGT values (pg cm-2 s-1), whereas Mg and Fe images show 13C-normalized intensities. Scale bar represents*

1 cm. Adapted from A. Kreuzeder, et al. 48. (B) Distribution of Mn, Fe, Zn, Cd and Pb around a S. smithiana root grown in soil moderately contaminated with Zn, Cd and Pb. Cationic trace metal solutes were sampled using HR-CBG for 20 h at a soil water saturation of ~80 % WHC. All images are displayed as calibrated fDGT values (pg cm-2 s-1). Scale bar represents 0.5 mm. Adapted from C. Hoefer, J. Santner, M. Puschenreiter and W. W. Wenzel 3. (C) Distribution of pH and multiple cationic solutes around S. smithiana roots grown in soil spiked with Cd. Co-localization of pH and solute dynamics was achieved using a modification of the HR-MBG protocol, allowing for simultaneous solute sampling and planar optode imaging33. The Mn, Cu, Zn and Cd images are displayed as calibrated fDGT values (pg cm-2 s-1), whereas Fe, Co, Ni and Pb images show 13C-normalized intensities. Scale bar represents 1 cm. Adapted from C. Hoefer, J. Santner, S. M. Borisov, W. W. Wenzel and M. Puschenreiter 33. The presented figures are reproduced from the cited articles3,33,48 licensed under CC BY."

Reviewer #4

Manuscript Summary:
The manuscript describes a method for visualizing the flow of plant nutrients and contaminants in soils using diffusive gradients in thin films and LA-ICP-MS. The method is well described and detailed, and the results are interesting.

Major Concerns:
None.

Thank you for the positive feedback.

Minor Concerns:
Line 746. I believe that the authors meant "less compacted" than "compacted less".

Thank you. The grammatical typo was **corrected**.

References used in this response letter

Davison, W., 2016. Diffusive Gradients in Thin-Films for Environmental Measurements. Cambridge University Press, Cambridge.

Gao, Y., Lehto, N., 2012. A simple laser ablation ICPMS method for the determination of trace metals in a resin gel. Talanta 92, 78-83.

Gonzalez, J., Mao, X.L., Roy, J., Mao, S.S., Russo, R.E., 2002. Comparison of 193, 213 and 266 nm laser ablation ICP-MS. Journal of Analytical Atomic Spectrometry 17, 1108-1113.

Guan, D.-X., Williams, P.N., Luo, J., Zheng, J.-L., Xu, H.-C., Cai, C., Ma, L.Q., 2015. Novel Precipitated Zirconia-Based DGT Technique for High-Resolution Imaging of Oxyanions in Waters and Sediments. Environmental Science & Technology 49, 3653-3661.

Guillong, M., Horn, I., Günther, D., 2003. A comparison of 266 nm, 213 nm and 193 nm produced from a single solid state Nd:YAG laser for laser ablation ICP-MS. Journal of Analytical Atomic Spectrometry 18, 1224-1230.

Günther, D., A. Heinrich, C., 1999. Enhanced sensitivity in laser ablation-ICP mass spectrometry using helium-argon mixtures as aerosol carrier. Journal of Analytical Atomic Spectrometry 14, 1363-1368.

Hoefer, C., Santner, J., Puschenreiter, M., Wenzel, W.W., 2015. Localized metal solubilization in the rhizosphere of Salix smithiana upon sulfur application. Environmental Science & Technology 49, 4522-4529.

Hooda, P.S., Zhang, H., Davison, W., Edwards, A.C., 1999. Measuring bioavailable trace metals by diffusive gradients in thin films (DGT): soil moisture effects on its performance in soils. European Journal of Soil Science 50, 285-294.

Ilhardt, P.D., Nuñez, J.R., Denis, E.H., Rosnow, J.J., Krogstad, E.J., Renslow, R.S., Moran, J.J., 2019. High-resolution elemental mapping of the root-rhizosphere-soil continuum using laser-induced breakdown spectroscopy (LIBS). Soil Biology and Biochemistry 131, 119-132.

Kreuzeder, A., Santner, J., Prohaska, T., Wenzel, W.W., 2013. Gel for simultaneous chemical imaging of anionic and cationic solutes using diffusive gradients in thin films. Anal Chem 85, 12028-12036.

Kreuzeder, A., Santner, J., Scharsching, V., Oburger, E., Hoefer, C., Hann, S., Wenzel, W.W., 2018. In situ observation of localized, sub-mm scale changes of phosphorus biogeochemistry in the rhizosphere. Plant and Soil.

Kreuzeder, A., Santner, J., Zhang, H., Prohaska, T., Wenzel, W.W., 2015. Uncertainty evaluation of the diffusive gradients in thin films technique. Environ Sci Technol 49, 1594-1602.

Lehto, N.J., Davison, W., Zhang, H., 2012. The use of ultra-thin diffusive gradients in thin-films (DGT) devices for the analysis of trace metal dynamics in soils and sediments: a measurement and modelling approach. Environmental Chemistry 9, 415-423.

Lehto, N.J., Larsen, M., Zhang, H., Glud, R.N., Davison, W., 2017. A mesocosm study of oxygen and trace metal dynamics in sediment microniches of reactive organic material. Scientific Reports 7, 11369.

Luo, Y., Gao, S., Longerich, H.P., Günther, D., Wunderli, S., Yuan, H.-L., Liu, X.-M., 2007. The uncertainty budget of the multi-element analysis of glasses using LA-ICP-MS. Journal of Analytical Atomic Spectrometry 22, 122-130.

Luster, J., Göttlein, A., Nowack, B., Sarret, G., 2009. Sampling, defining, characterising and modeling the rhizosphere—the soil science tool box. Plant and Soil 321, 457-482.

Oburger, E., Schmidt, H., 2016. New Methods To Unravel Rhizosphere Processes. Trends Plant Sci 21, 243-255.

Santner, J., Larsen, M., Kreuzeder, A., Glud, R.N., 2015. Two decades of chemical imaging of solutes in sediments and soils--a review. Anal Chim Acta 878, 9-42.

Santner, J., Williams, P.N., 2016. Measurement at High Spatial Resolution. In: Davison, W. (Ed.), Diffusive Gradients In Thin-Films For Environmental Measurements. Cambridge University Press, Cambridge, 174-215.

Smolders, E., Wagner, S., Prohaska, T., Irrgeher, J., Santner, J., 2020. Sub-millimeter distribution of labile trace element fluxes in the rhizosphere explains differential effects of soil liming on cadmium and zinc uptake in maize. Science of The Total Environment 738, 140311.

Wagner, S., Hoefer, C., Puschenreiter, M., Wenzel, W.W., Oburger, E., Hann, S., Robinson, B., Kretzschmar, R., Santner, J., 2020. Arsenic redox transformations and cycling in the rhizosphere of Pteris vittata and Pteris quadriaurita. Environmental and Experimental Botany 177, 104122.

Walas, S., Miliszkiewicz, N., Telk, A., 2014. Current approaches to calibration in LA-ICP-MS analysis. J. Anal. At. Spectrom. 30.

Warnken, K.W., Zhang, H., Davison, W., 2004a. Analysis of Polyacrylamide Gels for Trace Metals Using Diffusive Gradients in Thin Films and Laser Ablation Inductively Coupled Plasma Mass Spectrometry. Analytical Chemistry 76, 6077-6084.

Warnken, K.W., Zhang, H., Davison, W., 2004b. Performance characteristics of suspended particulate reagent-iminodiacetate as a binding agent for diffusive gradients in thin films. Anal Chim Acta 508, 41-51.

Williams, P.N., Santner, J., Larsen, M., Lehto, N.J., Oburger, E., Wenzel, W., Glud, R.N., Davison, W., Zhang, H., 2014. Localized flux maxima of arsenic, lead, and iron around root apices in flooded lowland rice. Environmental Science & Technology 48, 8498-8506.

SUPPORTING INFORMATION

Two-dimensional visualization and quantification of labile, inorganic plant nutrients and contaminants in soil

Stefan Wagner[1], Christoph Hoefer[2], Thomas Prohaska[1], Jakob Santner[1,3,*]

[1]Department General, Analytical and Physical Chemistry, Chair of General and Analytical Chemistry, Montanuniversität Leoben, Franz-Josef-Straße 18, 8700 Leoben, Austria.
[2]Department of Forest and Soil Sciences, Institute of Soil Research, University of Natural Resources and Life Sciences, Rhizosphere Ecology and Biogeochemistry Group, Vienna, Konrad-Lorenz-Straße 24, 3430, Tulln, Austria.
[3]Department of Crop Sciences, Institute of Agronomy, University of Natural Resources and Life Sciences, Vienna, Konrad-Lorenz-Straße 24, 3430 Tulln, Austria.

Email addresses of co-authors:
Stefan Wagner (stefan.wagner@unileoben.ac.at)
Christoph Hoefer (christoph.hoefer@gmail.com)
Thomas Prohaska (thomas.prohaska@unileoben.ac.at)

Corresponding author:
Jakob Santner (jakob.santner@boku.ac.at)

S1. Laboratory procedures for trace element analysis

S1.1. Use laboratory water type 1 with a conductivity of ≤0.055 µS cm^{-1} at 25 °C (**Table of Materials**) for all experimental procedures and solutions.

S1.2. Use chemical reagents of analytical grade or higher for all experiments.

S1.3. Acid-clean all glassware and plastics used for DGT gel preparation and application by soaking for 24 h in 10 % (*w*/*w*) HNO_3 (**Table of Materials**) followed by rinsing at least three times with H_2O. Acid-cleaned glassware and plastics must only get in contact with metal-free materials to avoid contamination.

S1.4. Perform all DGT gel coating and handling in a laminar flow bench (**Table of Materials**) or any other dust- and metal-free environment.

S2. Fabrication of DGT gels

S2.1. Polyurethane-based mixed anion and cation binding gel (HR-MBG)[1]

S2.1.1. Pre-clean HydroMed D4 (**Table of Materials**) by washing in H_2O (1:15, *w*/*v*) for ≥120 h using an overhead shaker (**Table of Materials**) at ~5 rpm. Change the H_2O ≥4 times during this period. Dry the pre-cleaned HydroMed D4 at 80 °C for 15 h and compensate the net weight loss compared to the initial material weight by adding H_2O.

S2.1.2. Cut 8 g of pre-cleaned HydroMed D4 to ~5 mm pieces and dissolve in 80 mL of an ethanol (**Table of Materials**)-water solution (10:1, *v*/*v*) using an overhead shaker at ~5 rpm overnight to get the polyurethane gel stock solution.

S2.1.3. Prepare 500 mL of 0.042 mol L^{-1} $ZrOCl_2 \times 8H_2O$ (**Table of Materials**) in a 1 L beaker. Place the beaker on a magnetic stirrer (**Table of Materials**) at ~300 rpm and immerse a calibrated pH probe (**Table of Materials**) connected to a pH meter (**Table of Materials**) into the solution.

S2.1.4. Titrate with 0.1 mol L^{-1} NaOH (**Table of Materials**) under vigorous stirring until the pH stabilizes at 7.0.

S2.1.5. Filter the $Zr(OH)_4$ precipitate using a vacuum flask connected to a vacuum pump and equipped with a Buechner funnel (**Table of Materials**) with quantitative filter paper (**Table of Materials**). Rinse with ~3 L of H_2O and filter until excess H_2O is removed and a hydrous $Zr(OH)_4$ slurry is obtained (**Figure S1A**).

NOTE: Do not filter until the slurry falls completely dry and forms cracks.

S2.1.6. Transfer 15 g (wet weight) $Zr(OH)_4$ precipitate slurry into a 120 mL vial and add the polyurethane gel stock solution (prepared in S2.1.2) to give a total volume of 100 mL $Zr(OH)_4$ precipitate-polyurethane suspension.

S2.1.7. Mix and homogenize the $Zr(OH)_4$ precipitate-polyurethane suspension using a dispersion device (**Table of Materials**) for 5-10 min at 20,000 rpm (**Figure S1B**).

NOTE: Take apart and clean the dispersion device using ethanol immediately after deployment, as rapid setting of the $Zr(OH)_4$ precipitate-polyurethane suspension can result in damage of the components.

S2.1.8. Mix 9 mL of the homogenized $Zr(OH)_4$ precipitate-polyurethane suspension with 1 mL of suspended particulate reagent iminodiacetic acid (SPR-IDA) (**Table of Materials**).

S2.1.9. Homogenize the viscous gel suspension via vigorous shaking by hand followed by slow agitation in an overhead shaker at ~5 rpm for ≥2 h to remove air bubbles and get the final gel suspension (**Figure S1C**).

S2.1.10. Fix 0.25 mm-thin PTFE spacer strips (**Table of materials**) left and right on a glass plate (25 cm x 18 cm) using adhesive tape. Place a knife-coating device (**Table of Materials**) on the top end of the glass plate onto the spacer strips.

S2.1.11. Pipette 3-4 mL of bubble-free gel suspension as a homogeneous 1-2 cm-wide wet film on the top end of the glass plate between the spacer strips (**Figure S1D**). Immediately, coat the wet film in a continuous motion from top to bottom of the glass plate using the knife-coating device (**Figure S1E**).

S2.1.12. Place the glass plate into an oven at 65 °C until the solvent is evaporated (~10 min). Afterwards, remove the glass plate from the oven and allow to cool to room temperature.

S2.1.13. Repeat S2.1.11 - S2.1.12 two more times to obtain a triple-layer gel coating on the glass plate.

S2.1.14. Remove the spacer strips and carefully remove areas with inhomogeneous distribution of the $Zr(OH)_4$ and SPR-IDA binding phases at the outer (~2 cm) edges of the gel coating using PTFE-coated razor blades (**Figure S1F**).

S2.1.15. Immerse the glass plate in ≥1 L H_2O in a plastic container until the gel detaches by hydration. Subsequently, remove the glass plate from the H_2O container.

NOTE: If the gel does not detach from the glass plate by itself after ~3 h of hydration, the gel needs to be carefully detached manually using plastic tweezers.

S2.1.16. Hydrate the gel in the H_2O bath for 24 h at room temperature. Exchange the H_2O at least

three times within 24 h to remove excess reagents from the gels.

S2.1.17. Store the hydrated 0.1 mm-thin HR-MBG in H_2O at 6 °C. The shelf life of the HR-MBG is 47 days.

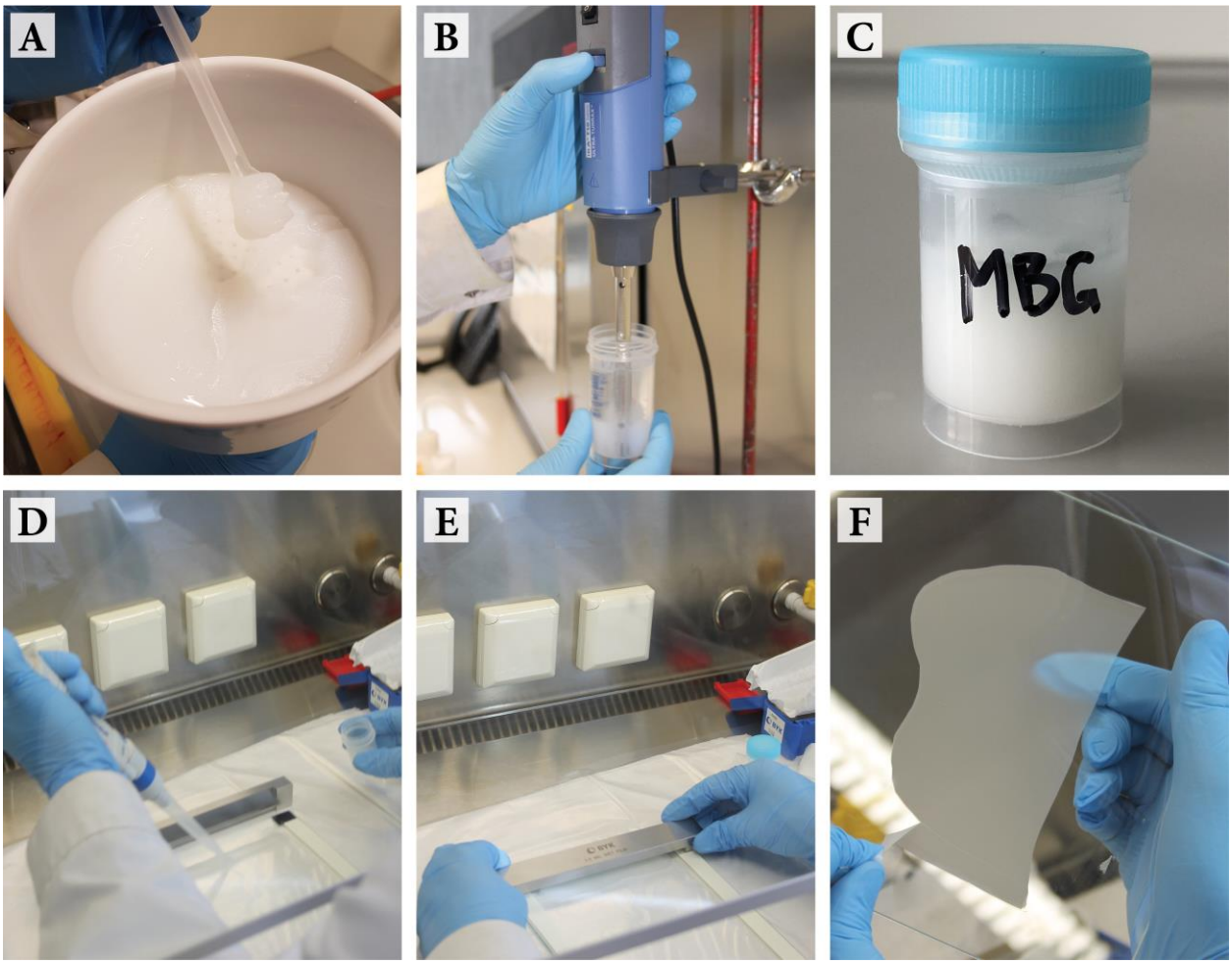

Figure S1: Fabrication of a HR-MBG for simultaneous sampling of anionic and cationic solutes. **(A)** $Zr(OH)_4$ slurry after filtration of the $Zr(OH)_4$ precipitate in a Buechner funnel. (**B**) Homogenization of the $Zr(OH)_4$ precipitate-polyurethane suspension using a dispersion device. (**C**) HR-MBG gel suspension in storage vial. (**D**) PTFE spacer strips are fixed left and right on a glass plate, the knife-coating device is placed on the top end of the glass plate, and the prepared gel suspension is pipetted as a thin film in front of the knife-coating device. (**E**) The knife-coating device is moved downwards to spread the gel suspension as a thin film on the glass plate. (**F**) Removal of gel areas with inhomogeneous material distribution before gel hydration.

S2.2. Polyacrylamide-zirconia anion binding gel (HR-ABG)[2]

S2.2.1. Prepare four 0.4 mm-thin APA gels as stated in S2.4.

S2.2.2. Prepare 40 mL of 0.45 mol L^{-1} $ZrOCl_2 \times 8H_2O$ (**Table of Materials**) in a 250 mL beaker.

S2.2.3. Immerse the four 0.4 mm-thin APA gels prepared in S2.2.1. into this solution and top up to a total volume of 100 mL (including the gels).

S2.2.4. Let the gels equilibrate for ≥2 h in the solution.

S2.2.5. Transfer each gel into 100 mL 0.05 mol L^{-1} 2-(N-morpholino)-ethanesulfonic acid (MES) (**Table of Materials**) buffer at pH 6.7. Immediately, stir the gel and solution using plastic tweezers during the first 60 s of immersion to ensure homogeneous precipitation of $Zr(OH)_4$ phases in the gel.

S2.2.6. Gently shake the vial containing the gel for a total of ~40 min to allow complete precipitation of $Zr(OH)_4$ in the gel.

S2.2.7. Remove the gel from the buffer and wash in ≥1 L H_2O for 24 h. Change the H_2O 5-6 times during this period to remove Cl^- ions and excess reagents.

S2.2.8. Store the hydrated 0.4 mm-thin HR-ABG in H_2O at 6 °C. The shelf life of the HR-ABG is ~13 months.

S2.3. Polyacrylamide-iminodiacetate cation binding gel (HR-CBG)[3]

S2.3.1. Mix 5.00 mL acrylamide (40 %; **Table of Materials**) and 1.25 mL DGT cross-linker (2 %; **Table of Materials**) to get the acrylamide gel stock solution.

CAUTION: Concentrated acrylamide solution is a classified toxin and suspected human carcinogen[4]. Do not inhale vapors, handle with gloves and follow general toxin reporting and safety requirements.

S2.3.2. Mix 1 mL of the acrylamide gel stock solution with 1 mL of suspended particulate reagent - iminodiacetate (SPR-IDA) resin suspension in a 20 mL vial to obtain a 5 % (*w*/*v*) resin-solution gel suspension.

NOTE: Vortex-mix the SPR-IDA resin suspension prior to pipetting.

S2.3.3. Homogenize the viscous gel suspension via vigorous shaking by hand followed by slow agitation in an overhead shaker at ~5 rpm for ≥2 h to remove air bubbles.

S2.3.4. Prepare a two-layer glass plate assembly separated by a U-shaped 0.25 mm-thin PTFE spacer for subsequent gel casting.

S2.3.5. Dissolve 0.1 g $(NH_4)_2S_2O_8$ (**Table of Materials**) in 1 mL of H_2O to get a 10 % (*w*/*v*)

ammonium persulfate (APS) solution required for subsequent gel polymerization.

NOTE: The APS solution must be prepared immediately prior gel fabrication.

S2.3.6. Add 14 µL APS and 4 µL of N,N,N',N'-tetramethylethylenediamine (TEMED; **Table of Materials**) to the air-bubble-free gel suspension and mix well using the pipette.

NOTE: Immediately proceed with S2.3.7, as gel polymerization is initiated rapidly following APS and TEMED addition.

S2.3.7. Pipette 2 mL of this gel suspension into the middle of the glass plate assembly using a 1 mL pipette tip. Hold the glass plate assembly almost vertical during pipetting to enable degassing of air-bubbles.

NOTE: Do not knock on the glass plate to remove air-bubbles, as this will result in inhomogeneous distribution of the iminodiacetate phases in the gel.

S2.3.8. Place the glass plate assembly containing the gel solution into an oven for 45 min at 45 °C until the gel is completely polymerized.

S2.3.9. Take the glass plate assembly apart. Therefore, remove the plastic clips and carefully lever up the top glass plate using e.g. a razor blade. The gel stays on the bottom glass plate.

NOTE: The application of H_2O between the two glass plates using a spray bottle will help to lever up the top glass plate without damaging the gel.

S2.3.10. Remove the U-shaped PTFE spacer and rinse the gel from the bottom glass plate into a suitable container filled with ≥1 L of H_2O using an H_2O spray bottle.

S2.3.11. Hydrate the gel in the H_2O bath for 24 h at room temperature. Exchange the H_2O at least three times during this period to remove excess reagents from the gel.

S2.3.12. Store the hydrated 0.4 mm-thin HR-CBG in H_2O at 6 °C. The shelf life of the HR-CBG is ~3 months.

S2.4. Agarose cross-linked polyacrylamide gel (APA)[5]

S2.4.1. Mix 5.00 mL acrylamide (40 %; **Table of Materials**), 2.00 mL DGT cross-linker (2 %; **Table of Materials**) and 6.33 mL H_2O to get the acrylamide gel stock solution.

S2.4.2. Prepare a two-layer glass plate assembly separated by a U-shaped PTFE spacer for subsequent gel casting. Use a PTFE spacer thickness of 0.25 mm or 0.50 mm for preparing a 0.4 mm-thin or 0.8 mm-thin APA, respectively.

S2.4.3. Prepare an APS solution as described in S2.3.5.

NOTE: The APS solution must be prepared immediately prior gel fabrication.

S2.4.4. For 0.4 mm-thin APA, pipette 2 mL of the acrylamide gel stock solution into a 20 mL vial and add 14 µL APS and 5 µL TEMED (**Table of Materials**) and mix well using the pipette. For 0.8 mm-thin APA, use twice the amount of the reagents.

NOTE: Immediately proceed with S2.4.5, as gel polymerization is initiated rapidly following APS and TEMED addition.

S2.4.5. Pipette 2 mL for 0.4 mm-thin APA or 4 mL for 0.8 mm-thin APA of this acrylamide gel solution into the glass plate assembly.

NOTE: If air bubbles appear, they can be removed by knocking on the glass plate using e.g. a pen.

S2.4.6. Proceed as detailed in S2.3.8 - S2.3.11 for gel polymerization and hydration.

S2.4.7. Store the hydrated APA (0.4 mm- or 0.8 mm-thin) in 0.01 mol L^{-1} $NaNO_3$ at 6°C. The shelf life of the APA is ~12 months.

S3. Plant cultivation

S3.1. Rhizotron design

S3.1.1. Manufacture rhizotron frames (**Figure 1A)** made from clear acrylic with inner dimensions of 40 cm × 10 cm × 1.5 cm (H × W × D). Use a thickness of 0.5 cm and 1.0 cm for the side and back walls, respectively.

S3.1.1.1. For the front (root viewing window), manufacture a 41 cm × 11 cm acrylic plate with 0.5 cm thickness which is attached to the rhizotron by 2 acrylic rails fixed by 4 nylon screws each alongside the side walls (**Figure 1A**).

S3.1.1.2. In the back, drill 14 holes with a diameter of ~5 mm to enable watering of the soil inside the rhizotron (**Figure 1A**). The watering holes can be closed using adhesive tape when not in use.

S3.1.2. Manufacture a tool for compacting the soil inside the rhizotron (**Figure 2B**). The compaction tool is made from an acrylic block with dimensions of 13 cm × 5 cm × 1.5 cm (H × W × D).

S3.1.3. Manufacture eight small 5 cm × 11 cm acrylic plates with 0.5 cm thickness. The plates are required for filling soil into rhizotrons (**Figure 2C**).

S3.2. Soil preparation before filling into the rhizotron

S3.2.1. Spread a thin (~3-5 cm) layer of air-dried and ≤2 mm-sieved soil into a plastic box.

S3.2.2. Moisten the soil surface with a H_2O spray bottle. The soil should be moist, but not saturated. Spread more soil layers on top and moisten them by spraying. Mix the soil by hand avoiding the formation of clumps. Repeat the procedure until the soil can be compacted in the fist and does not fall apart by itself.

S3.2.3. Sieve the soil one more time to ≤2 mm to remove larger aggregates. Dry a subsample (~50 g) at 105 °C for 24 h to determine the gravimetric water content, w_{soil} (g g^{-1}), according to Eq. S1. Typical w_{soil} values for rhizotron filling are between 0.05-0.15 g g^{-1} depending on the soil (particularly its clay content).

(Eq. S1) $w_{soil} = \frac{m_{w,soil}}{m_{s,soil}}$

Here, $m_{w,soil}$ (g) is the mass of water in the soil sample and $m_{s,soil}$ (g) is the mass of solids in the soil sample.

NOTE: It is recommended to equilibrate the pre-moistened soil for ~1 week at room temperature before filling into the rhizotron. Filling with (air-)dry soil is not recommended as this can result in the formation of cracks in the soil column following irrigation.

S4. Preparation of DGT LA-ICP-MS calibration standards

S4.1. Estimation of the analyte calibration range

S4.1.1. Conduct a preliminary DGT bulk soil experiment at the same conditions (i.e. temperature, soil water content, deployment time, material diffusion layer) as planned for the imaging experiment using conventional DGT bulk soil sampling procedures as described elsewhere[6,7].

NOTE: For DGT bulk soil sampling, assemble DGT samplers as detailed in S4.3, but replace the APA gel and polyethersulfone membrane (**Table of Materials**) with a polycarbonate membrane (**Table of Materials),** which is the sole material diffusion layer in DGT solute imaging experiments. Use a PTFE spacer (**Table of Materials**) at the bottom of the stack to compensate for the missing two layers.

S4.1.2. After bulk soil DGT sampling, retrieve the binding gel disc from the DGT sampler, rinse the gel thoroughly with water and recover the bound analytes from the gel via microwave assisted acid digestion or elution, depending on the binding gel used (see S4.4 for detailed procedures).

S4.1.3. Quantify the analyte concentration in the gel digest or eluate by a suitable analytical

technique (e.g. ICP-MS, colorimetry) and calculate the bound mass of analyte per gel area, Γ_{DGT} (gel analyte loading; µg cm^{-2}), according to Eq. S2.

(Eq. S2) $\Gamma_{DGT} = \frac{m_a}{A_p} = \frac{c_e \times (V_e + V_{bg})}{A_p \times f_e}$

Here, m_a (µg) is the mass of analyte accumulated on the binding gel, A_p (cm^2) is the area of the DGT sampler exposure window, c_e (µg L^{-1}) is the analyte concentration in the gel digest or eluate, V_e (L) is the volume of the digest or eluate solution, V_{bg} (L) is the volume of the binding gel, and f_e is the analyte- and binding gel-specific elution factor.

NOTE: Binding gel- and analyte-specific elution factors for HR-ABG and HR-CBG can be found in the original gel characterization publications[2,3].

S4.1.4. Define the highest calibration standard Γ_{DGT} for each analyte based on the determined and/or expected Γ_{DGT}.

S4.1.5. Verify that the total gel analyte loading (i.e. $\sum \Gamma_{DGT}$) of the highest calibration standard is well below the total analyte binding gel capacity (≤80 %).

NOTE: Gel- and analyte-specific binding capacities for the presented DGT binding gel types can be found in the original gel characterization publications[1-3].

S4.1.6. Divide the Γ_{DGT} of the highest calibration standard by the target number of calibration standards for each analyte. This will give the lowest calibration standard Γ_{DGT} and the distance between each standard to obtain an equidistant calibration series.

S4.1.7. If required, adjust the number of calibration points and/or the gel analyte loading of individual standards to encompass the expected gel analyte loading range.

S4.2. Preparation of the standard immersion solution

S4.2.1. Calculate the standard immersion solution analyte concentration corresponding to the target standard gel analyte loading derived from the calibration range estimated in section S4.1. In well-stirred solutions, a simple relationship between the actual analyte concentration in solution, c_{soln} (µg L^{-1}), and the analyte concentration measured by DGT samplers, c_{DGT} (µg L^{-1}), can be established[8]:

(Eq. S3) $c_{soln} = c_{DGT} = \Gamma_{DGT} \times \frac{\Delta g}{t \times D}$

Here, Δg (cm) is the total thickness of the material diffusion layer (i.e. APA gel and polyethersulfone membrane), *t* (s) is the deployment time of the DGT sampler, and *D* (cm^2 s^{-1}) is the diffusion coefficient of the analyte in the APA at a specific temperature[9].

NOTE: Eq. S3 defines a linear relationship between the deployment time t and the gel analyte loading Γ_{DGT}. Thus, increasing Γ_{DGT} can be obtained by increasing t at a constant c_{soln}. For the preparation of multi-point gel calibration standards, it is therefore recommended to use different sampler deployment times t in the same immersion solution rather than preparing individual immersion solutions with different c_{soln} for each gel standard.

S4.2.2. Prepare single-element standard stock solutions of the analytes by dissolving appropriate amounts of analytical grade analyte salts (**Table of Materials**) to obtain adequate stock solution concentrations (typically between 100-500 mg L^{-1}).

CAUTION: Pay attention to safety regulations as most metal compounds are potentially toxic.

S4.2.3. Dissolve 297.5 mg $NaNO_3$ in 2 L H_2O in a 3.5 L plastic container. Place the beaker on a magnetic stirrer (**Table of Materials**) at ~300 rpm and immerse a calibrated pH probe (**Table of Materials**) connected to a pH meter (**Table of Materials**).

S4.2.4. Add an appropriate volume of each single-element standard stock solution to the well-stirred immersion solution to give the target analyte concentration in solution, c_{soln}, considering a total volume of the final immersion solution of 3 L.

NOTE: Pay attention to analyte-specific precipitation and complexation reactions, formation of colloidal species, and sorption to the container walls to make sure that analyte concentrations in solution remain constant over the experimental deployment period. If multi-analyte solutions are used, it is recommended to calculate the solubility equilibria using chemical equilibrium modelling software (**Table of Materials**).

S4.2.5. Adjust the pH of the immersion solution to ~5.6 using 0.1 mol L^{-1} NaOH or 0.1 mol L^{-1} HNO_3.

S4.2.6. Top up the immersion solution volume to 3 L with H_2O and let the immersion solution equilibrate for ≥12 h under constant stirring. Close the plastic container to avoid contamination and evaporation.

S4.2.7. Verify that the pH remained constant at ~5.6 upon equilibration.

S4.2.8. Sample an aliquot (5-10 mL) from the immersion solution to assess the initial analyte concentration in solution by e.g. ICP-MS.

S4.3. Standard gel loading

S4.3.1. Cut the DGT binding gels to individual discs with 2.5 cm diameter using a circular cutter made from either stainless-steel (**Table of Materials**) for HR-MBG and HR-ABG, or plastic (**Table of Materials**) for HR-CBG.

S4.3.2. Assemble standardized DGT piston samplers (**Table of Materials**) by stacking a binding gel disc, a 0.8 mm-thin APA diffusive gel (see S2.4 for fabrication details), and a 0.14 mm-thin polyethersulfone membrane (0.45 µm pore size; **Table of Materials**) on top of each other on the DGT base (**Figure S2**) using plastic tweezers. Apply water to facilitate positioning of the individual layers and ensure that no air bubbles are trapped between the layers and that each layer is centered on the DGT base.

NOTE: If HR-MBG is used, add a 0.4 mm-thin PTFE support at the DGT base to compensate for the lower gel thickness of the HR-MBG as compared to HR-ABG and HR-CBG.

S4.3.3. Close the DGT piston sampler with the DGT cap. Press the cap until the DGT sampler is tightly sealed and verify that the polyethersulfone membrane is flat and not damaged.

S4.3.4. Assemble four DGT piston sampler replicates per gel standard or blank. The samplers can be stored for a few days in a zip bag containing a few mL of water at 6 °C in the fridge until deployment in the immersion solution.

NOTE: For the standard gel blank, skip S4.3.5 - S4.3.10 and directly proceed with S4.3.11.

S4.3.5. Fix each DGT piston sampler (four per gel standard) in a custom-built support frame and deploy the samplers in the well-stirred immersion solution (**Figure S2**).

S4.3.6. Record the exact starting time of the sampler deployment.

S4.3.7. Deploy the DGT piston samplers in the immersion solution until the end of the deployment time *t*.

S4.3.8. Retrieve the DGT samplers from the immersion solution and the support frame and rinse thoroughly with water.

S4.3.9. Record the exact end time of the DGT piston sampler deployment.

S4.3.10. Sample an aliquot from the immersion solution as specified in S4.2.8 to assess the final analyte concentration in solution.

S4.3.11. Retrieve the binding gel discs from the DGT samplers and rinse the gels thoroughly with water.

S4.3.12. Dry one of the four gel replicates per gel standard or blank as detailed in the main document section 3.3. This gel will serve as standard for LA-ICP-MS analysis (**Figure S2**).

S4.3.13. Transfer the remaining three gel replicates per gel standard or blank into a 20 mL storage vial pending gel digestion or elution for analyte quantification (**Figure S2**).

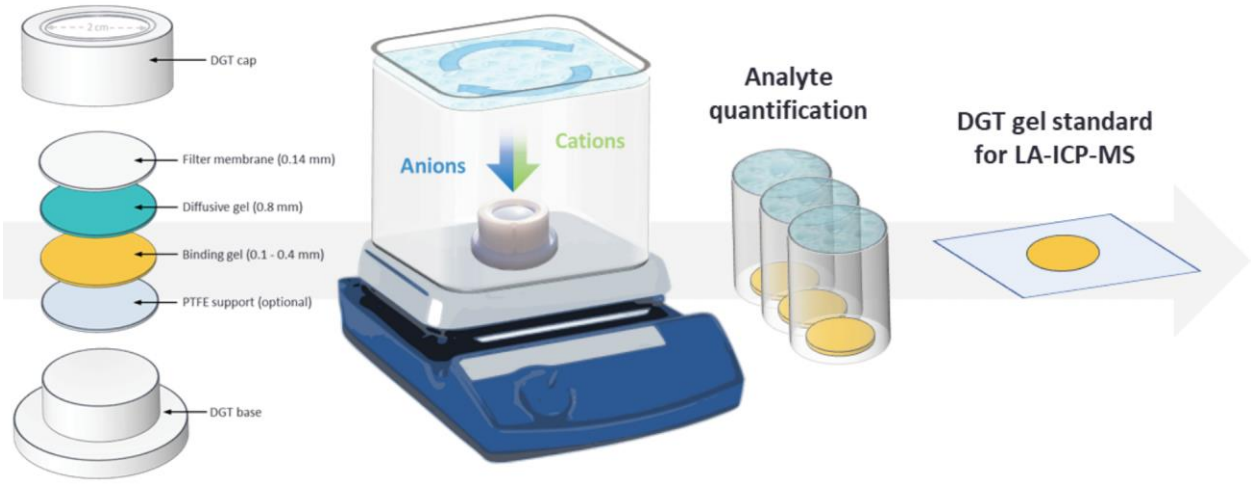

Figure S2: Laboratory workflow for the preparation of DGT LA-ICP-MS calibration standards.

S4.4. Standard gel digestion or elution

NOTE: Different procedures are applied to recover the bound analytes from the presented DGT binding gel discs. While the HR-MBG gel requires digestion for complete analyte recovery, HR-ABG and HR-CBG only need to be eluted.

S4.4.1. HR-MBG[1]

S4.4.1.1. Transfer the HR-MBG discs from the 20 mL storage vial into the vessels of a high-pressure microwave system (**Table of Materials**).

S4.4.1.2. Add 5 mL of 65 % (*w*/*w*) HNO_3 (**Table of Materials**) and 1 mL of 30 % (*w*/*w*) H_2O_2 (**Table of Materials**) to the gel discs and run the following settings on the microwave: Phase 1: power 1400 W, ramp 10 min, hold 60 min, fan 1; Phase 2: power 0 W, ramp 0 min, hold 5 min, fan 3.

S4.4.1.3. Dilute the digests to 2 % (*w*/*w*) HNO_3. If analyte concentrations are expected to be below <1 µg L^{-1}, matrix evaporation at 90 °C in perfluoroalkoxy alkane (PFA) vials (**Table of Materials**) may help to preconcentrate the analytes to reach ICP-MS detection limits.

S4.4.2. HR-ABG[2]

S4.4.2.1. Add 5 - 10 mL 0.5 mol L^{-1} NaOH directly to the HR-ABG discs in the 20 mL storage vial.

S4.4.2.2. Elute for ≥24 h under constant shaking on a horizontal shaker (**Table of Materials**).

S4.4.2.3. Retrieve the HR-ABG discs from the eluate and measure the analytes by ICP-MS or colorimetry.

S4.4.3. HR-CBG[3]

S4.4.3.1. Add 1 - 10 mL 1 mol L^{-1} HNO_3 directly to the HR-CBG discs in the 20 mL storage vial.

S4.4.3.2. Elute for ≥24 h under constant shaking on a horizontal shaker.

S4.4.3.3. Retrieve the HR-CBG discs from the eluate, dilute the eluates to 2 % (*w*/*w*) HNO_3 and measure the analytes by ICP-MS.

S5. Coupling the LA system to the ICP-MS

NOTE: The experimental system uses specific LA-ICP-MS instrumentation (**Figure 5**; **Table of Materials**). If systems from other manufacturers are used, modifications to the protocol may be required.

CAUTION: The LA system uses a class 4 laser which can cause severe injuries to skin and eyes and therefore requires proper safety management[10]. Conduct technical training before operation of the LA-ICP-MS instrumentation.

S5.1. Start the LA system and the ICP-MS instrument and perform a performance check on both systems according to the manufacturer's specifications.

NOTE: Stop the plasma on the ICP-MS after the performance check, i.e. before you connect the LA system.

S5.2. Connect N_2 as purge gas to 'N2 PRG GAS IN' and He as carrier gas to 'MFC 1 GAS IN' at the gas panel of the LA system. Verify that the gas properties (i.e. pressure and purity) are in line with the specifications of the LA system.

NOTE: The present protocol uses He as the aerosol carrier gas. Alternatively, Ar can be used as carrier gas. See Günther and Heinrich[11] for a detailed discussion of the effects of using either He or Ar as carrier gas.

S5.3. Connect the 'ONLINE GAS OUT' He carrier gas flow of the LA system and the 'NEB' Ar nebulizer gas flow of the ICP-MS to the ICP interface via a PTFE-coated Tygon tubing (**Table of Materials**) equipped with a two-way Y connector and a torch adapter fitting to the ICP injector (**Figure 5C**).

S5.4. Verify that all gas fittings are finger-tight, and that the tubing connection is sound and leak-free.

S5.5. Connect the 'SYNC OUT' port of the LA system to the 'I/O' port of the ICP-MS via a transistor-transistor logic (TTL) cable (**Table of Materials**) to trigger the ICP-MS data acquisition with the

LA. In the LA software, set the 'Sync Out Mode' to 'Active when Laser Active' and 'Sync Out Polarity' to 'Active Closed'. Set the ICP-MS 'Sampling Device' to 'External' and the 'External Read Trigger' to 'Close' in the ICP-MS software.

S5.6. Click 'N_2 Purge' in the LA software to purge the laser optics with N_2. Click 'Mass Flow' to open the 'Mass Flow Control' window, tick 'Enable flow controller' and set the carrier gas flow rate to 900 mL min^{-1}. Switch from 'Bypass' to 'Online' to purge the LA cell with the carrier gas for ≥30 min.

S5.7. Reduce the carrier gas flow to 0 mL min^{-1} and start the plasma in the ICP-MS software. Subsequently, slowly ramp up the carrier gas flow to the desired 900 mL min^{-1} at a ramp up rate of 10-20 mL min^{-1} s^{-1}.

NOTE: Closely monitor the plasma stability during the carrier gas ramp up to ensure that the plasma is not extinguished by the increase in gas flow and that the torch is not overheating.

S5.8. Once the plasma is stabilized (after ~30 min), monitor the gas blank in the ICP-MS in real-time until the analyzed isotopes reach a constant level prior to the start of the measurement.

NOTE: If high and/or strongly scattering gas blank levels are present, this may indicate leaks or contamination in the LA-ICP-MS tubing connection or the ablation cell, which then needs to be considered in detail.

S5.9. Proceed with LA-ICP-MS analysis as specified in the main document section 4.2.

REFERENCES

1 Kreuzeder, A., Santner, J., Prohaska, T. & Wenzel, W. W. Gel for simultaneous chemical imaging of anionic and cationic solutes using diffusive gradients in thin films. *Anal Chem.* **85** (24), 12028-12036, (2013).

2 Guan, D.-X. *et al.* Novel Precipitated Zirconia-Based DGT Technique for High-Resolution Imaging of Oxyanions in Waters and Sediments. *Environmental Science & Technology.* **49** (6), 3653-3661, (2015).

3 Warnken, K. W., Zhang, H. & Davison, W. Performance characteristics of suspended particulate reagent-iminodiacetate as a binding agent for diffusive gradients in thin films. *Anal Chim Acta.* **508** (1), 41-51, (2004).

4 International Agency for Research on Cancer. *IARC Monographs on the Evaluation of Carcinogenic Risks to Humans: Vol. 60 Some Industrial Chemicals*, <https://publications.iarc.fr/Book-And-Report-Series/Iarc-Monographs-On-The-Identification-Of-Carcinogenic-Hazards-To-Humans/Some-Industrial-Chemicals-1994> (1994).

5 Zhang, H. & Davison, W. Performance Characteristics of Diffusion Gradients in Thin Films for the in Situ Measurement of Trace Metals in Aqueous Solution. *Analytical Chemistry.* **67** (19), 3391-3400, (1995).

6 Hooda, P. S., Zhang, H., Davison, W. & Edwards, A. C. Measuring bioavailable trace metals by diffusive gradients in thin films (DGT): soil moisture effects on its performance in soils. *European Journal of Soil Science.* **50** (2), 285-294, (1999).

7 Smolders, E., Wagner, S., Prohaska, T., Irrgeher, J. & Santner, J. Sub-millimeter distribution of labile trace element fluxes in the rhizosphere explains differential effects of soil liming on cadmium and zinc uptake in maize. *Science of The Total Environment.* **738** 140311, (2020).

8 Davison, W. & Zhang, H. in *Diffusive Gradients In Thin-Films For Environmental Measurements* (ed William Davison) 10-31 (Cambridge University Press, 2016).

9 DGT Research. *Diffusion Coefficients*, <https://www.dgtresearch.com/diffusion-coefficients/> (2020).

10 Smalley, P. J. Laser safety: Risks, hazards, and control measures. *Laser Therapy.* **20** (2), 95-106, (2011).

11 Günther, D. & A. Heinrich, C. Enhanced sensitivity in laser ablation-ICP mass spectrometry using helium-argon mixtures as aerosol carrier. *Journal of Analytical Atomic Spectrometry.* **14** (9), 1363-1368, (1999).